

Nested Deep Learning Model Towards a Foundation Model for Brain Signal Data

Fangyi Wei¹, Jiajie Mo², Kai Zhang², Haipeng Shen¹, Srikantan
Nagarajan³, and Fei Jiang^{*4}

¹Innovation and Information Management, Faculty of Business and
Economics, The University of Hong Kong, China

²Department of Neurosurgery, Beijing Tiantan Hospital, China

³Department of Radiology, University of California, San Francisco

⁴Department of Epidemiology and Biostatistics, University of California,
San Francisco

Abstract

Epilepsy affects around 50 million people globally. Electroencephalography (EEG) or Magnetoencephalography (MEG) based spike detection plays a crucial role in diagnosis and treatment. Manual spike identification is time-consuming and requires specialized training that further limits the number of qualified professionals. To ease the difficulty, various algorithmic approaches have been developed. However, the existing methods face challenges in handling varying channel configurations and in identifying the specific channels where the spikes originate. A novel Nested Deep Learning (NDL) framework is proposed to overcome these limitations. NDL applies a weighted combination of signals across all channels, ensuring adaptability to different channel setups, and allows clinicians to identify key channels more accurately. Through theoretical analysis and empirical validation on real EEG/MEG datasets, NDL is shown to improve prediction accuracy, achieve channel localization, support cross-modality data integration, and adapt to various neurophysiological applications.

Keywords: epilepsy, Electroencephalography, spike detection, deep learning, neuroimaging.

*Email: fei.jiang@ucsf.edu

1 Introduction

Currently, around 50 million people worldwide suffer from epilepsy, one of the most common neurological diseases globally (World Health Organization 2024). Detecting epileptiform discharges, particularly spikes, during the interictal periods, plays a crucial role in the diagnosis of epilepsy.

Spikes are abnormal brain activities that typically occur intermittently and spontaneously, lasting around 100 to 250 milliseconds, in epilepsy patients. They can be measured with Electroencephalography (EEG) or Magnetoencephalography (MEG) devices. The devices collect brain signals through EEG or MEG sensors attached to different areas of the scalp and visualize the signals as time series waveforms. The EEG or MEG recordings then consist of multi-channel time series signal data. Identifying spikes not only helps predict the risk of seizures, but also helps localize the onset zone of seizures, which is critical for epilepsy surgery (Smith et al. 2022).

Thus, it becomes imperative to develop novel interpretable methods that can effectively identify spikes to assist clinical decisions. However, clinical practices predominantly employ manual identification of spikes, which is a labor-intensive process, especially when analyzing continuous or video EEG studies that can last more than 24 hours. Furthermore, this task requires specialized training, restricting the number of clinicians qualified to evaluate EEG studies, resulting in a significant shortage of neurologists trained in interpreting EEG data (Torres and Butter 1996).

To mitigate this issue, various algorithm-based methods have been proposed to automate the identification process. Lodder et al. (2013) adopt template matching to compare signal patterns with spike templates. Indiradevi et al. (2008) use wavelet transformation

to decompose spike signals. Baud et al. (2018) use an unsupervised learning approach to automate spike detection. With the advancement of deep learning, the field is increasingly adopting deep learning algorithms for spike detection. For example, Antoniadou et al. (2016), Johansen et al. (2016), Tjepkema-Cloostermans et al. (2018), Thomas et al. (2020), Clarke et al. (2021) and Chung et al. (2023) employ convolutional neural networks (CNNs) to classify abnormal and normal waveforms; Medvedev et al. (2019) use a Long Short-Term Memory neural network for the spike detection task.

Despite these developments, two significant challenges remain. Firstly, different studies have varying numbers and locations of the channels, as well as the montages used, all of which make it difficult to develop a universal algorithm that can accommodate all channel setups. For instance, Golmohammadi et al. (2019) develop an algorithm based on spikes labeled using the temporal central parasagittal montage with 22 channels, whereas Jing et al. (2020)'s algorithm is designed for the longitudinal bipolar montage with 18 channels and the common average reference montage with 19 channels. A general adaptive algorithm is crucial because it allows data integration between studies, thereby enhancing prediction accuracy. It also allows clinicians to choose their preferred montage for analysis.

Secondly, although current detection algorithms can identify time segments that contain spikes, they lack the ability to pinpoint the exact channels where the spikes originate. Identifying specific channels is crucial because it helps locate the seizure onset zone, helps clinicians review and validate detection results, and serves as a key factor in ruling out false detections in less likely channels.

We propose a novel nested deep learning framework (NDL) to address these challenges. For the first challenge, we propose a weight function for each channel, customized to its specific signal pattern within a given time range of interest, preferably less than one second.

Then we model the probability of a time segment to contain a spike via a weighted combination of signals across all channels. For the second challenge, these weights are designed to reflect the importance of each channel in terms of their relevance in the spike detection.

Our NDL approach is superior to the traditional channel-based methods (Wilson et al. 1999; Goelz et al. 2000), which require the tedious process of labeling each channel to achieve similar results. NDL offers a faster inference process that can handle large volumes of data simultaneously. Furthermore, NDL considers the signal information from all channels, which improves the prediction accuracy because there are often concurrent spikes that appear on multiple channels. Moreover, because NDL is invariant to channel configurations, it can serve as a foundational model for integrating neurophysiological data from various modalities and can be fine-tuned to adapt to different new tasks.

We apply NDL to three real datasets to evaluate its performance in Section 4. We start with a well-labeled EEG dataset from Temple University Hospital (TUH), focusing on its sensitivity and specificity in detecting spikes, as well as its accuracy in identifying the EEG channels where these spikes occur (Section 4.2). The dataset is the only public EEG dataset that provides not only the time label of spike occurrence but also the specific channels containing the spikes, as the ground truth for the evaluation. We then apply NDL to two private datasets: a 140-channel MEG dataset from the University of California, San Francisco (UCSF), and a 19-channel EEG dataset from China’s Beijing Tiantan Hospital (BTH). The results first demonstrate that the model trained on the UCSF MEG data performs well in detecting spikes and identifying relevant channels (Section 4.3). Furthermore, the MEG-trained model can even successfully detect spikes in the out-of-sample BTH EEG data, even though the testing data modality differs from the training data modality (Section 4.4). This study indicates that NDL has strong generalizability across different

datasets, even with varying numbers of channels. Finally, Section 4.5 proposes an algorithm that enables the application of NDL to continuous MEG/EEG recordings commonly available in practice.

The rest of the paper is presented as follows. We introduce the model in Section 2, and present the deep learning estimation procedure in Section 3. Besides the performance of NDL on the three real datasets and its comparison with existing methods in Section 4, we demonstrate its performance and convergence on simulated data in Section 5. Finally, we study the theoretical properties of the estimator in Section 6.

To facilitate the presentation, we define the following notations. The L_0 , L_1 , L_2 and the supremum norms of a vector \mathbf{v} are denoted by $\|\mathbf{v}\|_0$, $\|\mathbf{v}\|_1$, $\|\mathbf{v}\|_2$ and $\|\mathbf{v}\|_\infty$, respectively. Furthermore, for a given matrix \mathbf{M} , we denote the matrix entry-wise supremum norm, L_0 , L_1 , the operator norms as $\|\mathbf{M}\|_\infty$, $\|\mathbf{M}\|_0$, $\|\mathbf{M}\|_1$, and $\|\mathbf{M}\|_2$, respectively. For a function $f(\mathbf{x})$, we denote the functional supremum norm as $\|f(\mathbf{x})\|_\infty \equiv \sup |f(\mathbf{x})|$.

2 Model

Let $\mathbf{X}_i = \{\mathbf{X}_{il}, l = 1, \dots, d\}^\top$ be a random matrix representing a segment of multi-channel signals, where d is the number of channels, \mathbf{X}_{il} is a T -dimensional vector representing the signals in Channel l with T time measurements. We aim to predict whether the segment \mathbf{X}_i contains a spike or not. Let Y_i be a binary indicator, where $Y_i = 1$ indicates that a spike appears in at least one channel in the segment \mathbf{X}_i , and $Y_i = 0$ indicates that no spike appears in the segment. Furthermore, let $\mathbf{Z}_i = \{\mathbf{Z}_{il}, l = 1, \dots, d\}^\top$ represent a segment of background signals surrounding \mathbf{X}_i , where \mathbf{Z}_{il} is a p -dimensional vector containing signals from p time measurements in Channel l . We assume that $\{Y_i, \mathbf{X}_i, \mathbf{Z}_i\}$, $i = 1, \dots, n$, are independent identically distributed. Figure 1 provides two exemplary segments where $Y_i =$

0 and $Y_j = 1$, with the corresponding $\{\mathbf{X}_i, \mathbf{Z}_i\}$ and $\{\mathbf{X}_j, \mathbf{Z}_j\}$.

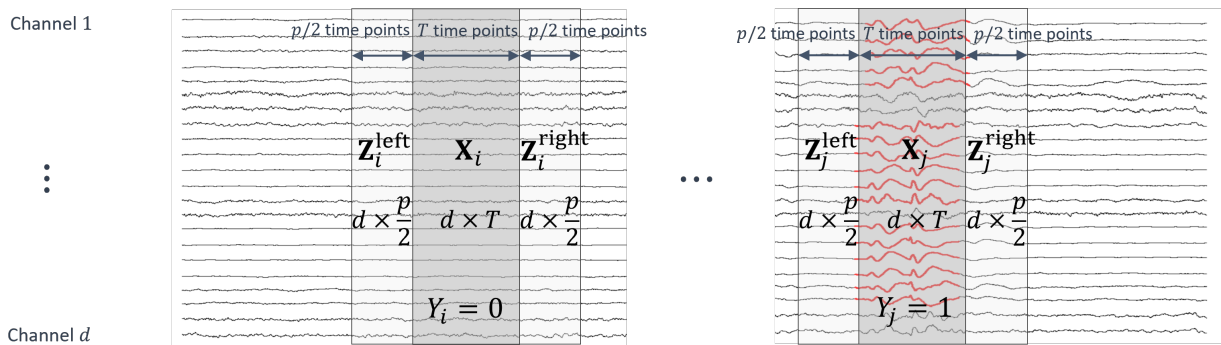


Figure 1: Illustration of $\{Y_i = 0, \mathbf{X}_i, \mathbf{Z}_i\}$ (left) and $\{Y_j = 1, \mathbf{X}_j, \mathbf{Z}_j\}$ (right). Spike signals are annotated in red and bold while background signals are shown in black. In the TUH data of Section 4.2, we set $d = 22$, $T = p = 250$.

We define a channel-specific weight function as $\boldsymbol{\alpha}(\mathbf{X}_{il}, \mathbf{X}_i) = \{\alpha_k(\mathbf{X}_{il}, \mathbf{X}_i), k = 1, \dots, p\}^\top$, where $\alpha_k(\mathbf{X}_{il}, \mathbf{X}_i) = \exp\{\omega_k(\mathbf{X}_{il})\} / \sum_{l=1}^d \exp\{\omega_k(\mathbf{X}_{il})\}$ represents the k -th weight, dynamically standardized across d channels. Here, $\omega_k(\mathbf{X}_{il})$, $k = 1, \dots, p$, are unknown real-valued functions. The weight function $\boldsymbol{\alpha}(\mathbf{X}_{il}, \mathbf{X}_i)$ incorporates information from all channels while placing particular emphasis on Channel l , highlighting the importance of signal patterns in that channel. Then we combine the signals including \mathbf{X}_i and \mathbf{Z}_i , through

$$\mathbf{S}_i(\boldsymbol{\alpha}) \equiv \sum_{l=1}^d \{\mathbf{X}_{il} \boldsymbol{\alpha}(\mathbf{X}_{il}, \mathbf{X}_i)^\top + \mathbf{1}_T \boldsymbol{\alpha}(\mathbf{X}_{il}, \mathbf{X}_i)^\top \mathbf{Z}_{il} \mathbf{1}_p^\top\}, \quad (1)$$

where $\mathbf{1}_T$ and $\mathbf{1}_p$ are T - and p - dimensional one vectors, respectively. We introduce an unknown real function $g(\cdot) : \mathbb{R}^{T \times p} \rightarrow \mathbb{R}$ to capture the complex relationship between the combination defined in (1) and the response Y_i . We then assume that the conditional probability for $Y_i = 1$ is in the following form:

$$\Pr(Y_i = 1 | \mathbf{X}_i, \mathbf{Z}_i) = \{1 + \exp[-g\{\mathbf{S}_i(\boldsymbol{\alpha})\}]\}^{-1}, \quad (2)$$

where g and $\boldsymbol{\alpha}$ are unknown functions that need to be estimated.

We make some remarks about the formulation (1) and Model (2). In (1), the first term $\sum_{l=1}^d \mathbf{X}_{il} \boldsymbol{\alpha}(\mathbf{X}_{il}, \mathbf{X}_i)^\top$ maps the signals \mathbf{X}_i from d channels onto a shared p -dimensional space. Intuitively, a higher value of $\|\boldsymbol{\alpha}(\mathbf{X}_{il}, \mathbf{X}_i)\|_2$ indicates a greater contribution of Channel l to the outcome. It is worth noting that using only this term makes the model unidentifiable because the order of the columns of $\boldsymbol{\alpha}(\mathbf{X}_{il}, \mathbf{X}_i)$ can vary arbitrarily. The second term $\sum_{l=1}^d \mathbf{1}_T \boldsymbol{\alpha}(\mathbf{X}_{il}, \mathbf{X}_i)^\top \mathbf{Z}_{il} \mathbf{1}_p^\top$ is introduced to address this problem. By multiplying each element of $\boldsymbol{\alpha}(\mathbf{X}_{il}, \mathbf{X}_i)$ with a distinct element of \mathbf{Z}_{il} , we effectively fix the order of the columns of $\boldsymbol{\alpha}(\mathbf{X}_{il}, \mathbf{X}_i)$, ensuring the identifiability of the model. We show that

Proposition 1 *Assume $g(\cdot)$ is continuously differentiable and $\sum_{l=1}^d \boldsymbol{\alpha}(\mathbf{X}_{il}, \mathbf{X}_i) = \mathbf{1}$. Then $\boldsymbol{\alpha}(\mathbf{X}_{il}, \mathbf{X}_i)$ and $g(\cdot)$ are identifiable.*

In the model, the dimension p , i.e. the dimension of \mathbf{Z}_{il} and the dimension of $\boldsymbol{\alpha}(\mathbf{X}_{il}, \mathbf{X}_i)$, should be selected appropriately depending on the context. When $p < T$, a low-dimensional embedding of the data is obtained, which can be beneficial for dimension reduction in analyses involving a large number of time points. This approach is particularly useful for tasks such as seizure detection or resting-state signal classification, where signal recordings span across minutes or hours. In contrast, when $p = T$, all the original signal information is preserved. This choice is recommended for tasks like spike detection, where the analysis involves only short data segments, typically containing less than 100 time points. We set $p = T$ for the real data analyses in this paper.

3 Deep Learning Estimation

Let g^* and $\boldsymbol{\alpha}^*$ denote the true functions for g and $\boldsymbol{\alpha}$ in Model (2), respectively. To flexibly capture the structures of the two unknown functions, we adopt deep neural networks with the ReLU activation function (Schmidt-Hieber 2020) to approximate g^* and $\boldsymbol{\alpha}^*$.

More specifically, let network architectures with L numbers of layers and a width vector \mathbf{p}_w , where $\mathbf{p}_w = (p_{w0}, \dots, p_{w(L+1)}) \in \mathbb{N}^{L+1}$, to represent any function in the form of

$$f : \mathbb{R}^{p_{w0}} \rightarrow \mathbb{R}^{p_{w(L+1)}}, \mathbf{x} \rightarrow f(\mathbf{x}) \equiv \mathbf{W}_L \sigma_{\mathbf{v}_L} \mathbf{W}_{L-1} \sigma_{\mathbf{v}_{L-1}}, \dots, \mathbf{W}_1 \sigma_{\mathbf{v}_1} \mathbf{W}_0 \mathbf{x}, \quad (3)$$

where $\sigma_{\mathbf{v}}(y_1, \dots, y_r) = \{\sigma(y_1 - v_1), \dots, \sigma(y_r - v_r)\}$ is a vector of ReLU activation functions, \mathbf{W}_i is a $p_{w(i+1)} \times p_{wi}$ weight matrix, and $\mathbf{v}_i \in \mathbb{R}^{p_{wi}}$ is a shift vector. Then we denote the set of these neural network functions with s numbers of nonzero parameters as

$$\mathcal{F}(L, \mathbf{p}_w, s, F) \equiv \left\{ f \text{ of the form (3)} : \max_{j=0, \dots, L} \max(\|\mathbf{W}_j\|_\infty, \|\mathbf{v}_j\|_\infty) \leq 1, \right. \\ \left. \sum_{j=1}^L \|\mathbf{W}_j\|_0 + \|\mathbf{v}_j\|_0 \leq s, \sup_{\mathbf{x}} |f(\mathbf{x})| \leq F \right\}.$$

Denote $\mathcal{F}_f = \mathcal{F}(L_f, \mathbf{p}_f, s_f, F_f)$, where f can be $g, \omega_k, k = 1, \dots, p$.

Furthermore, we define a general form of the true function space as follows.

Definition 1 Define the set of β -Hölder functions with radius K as

$$\mathcal{C}_t^\beta(D, K) \equiv \left\{ f : D \subset \mathbb{R}^t \rightarrow \mathbb{R} : \right. \\ \left. \sum_{\gamma: \|\gamma\|_1 < \beta} \|\partial^\gamma f\|_\infty + \sum_{\gamma: \|\gamma\|_1 = \lfloor \beta \rfloor} \sup_{\mathbf{x}_1, \mathbf{x}_2 \in D, \mathbf{x}_1 \neq \mathbf{x}_2} \frac{|\partial^\gamma f(\mathbf{x}_1) - \partial^\gamma f(\mathbf{x}_2)|}{\|\mathbf{x}_1 - \mathbf{x}_2\|_\infty^{\beta - \lfloor \beta \rfloor}} \leq K \right\},$$

where $\partial^\gamma = \partial^{\gamma_1} \dots \partial^{\gamma_t}$ with $\boldsymbol{\gamma} = (\gamma_1, \dots, \gamma_t)^\top \in \mathbb{N}^t$, and $\lfloor \beta \rfloor$ denotes the largest integer strictly smaller than β . Then the set of true function space is defined as

$$\mathcal{G}(q, \mathbf{d}, \mathbf{t}, \boldsymbol{\beta}, K) \equiv \left\{ f = g_q \circ \dots \circ g_0 : g_u \equiv (g_{uj})_j : [a_u, b_u]^{d_u} \rightarrow [a_{u+1}, b_{u+1}]^{d_{u+1}}, \right. \\ \left. g_{uj} \in \mathcal{C}_{t_u}^{\beta_u}([a_u, b_u]^{t_u}, K), \text{ for some } |a_i|, |b_i| < K \right\},$$

where $\mathbf{d} \equiv (d_0, \dots, d_{q+1})$, $\mathbf{t} \equiv (t_0, \dots, t_q)^\top$ and $\boldsymbol{\beta} \equiv (\beta_0, \dots, \beta_q)^\top$.

For notational convenience, we denote the true function space for an arbitrary function f as $\mathcal{G}_f \equiv \mathcal{G}(q_f, \mathbf{d}_f, \mathbf{t}_f, \boldsymbol{\beta}_f, K_f)$. Assume that $g^* \in \mathcal{G}_g, \omega_k^* \in \mathcal{G}_{\omega_k}$ are the true functions of g, ω_k .

Let $\alpha_k^*(\mathbf{X}_{il}, \mathbf{X}_i) = \exp\{\omega_k^*(\mathbf{X}_{il})\} / \sum_{l=1}^d \exp\{\omega_k^*(\mathbf{X}_{il})\}$ and $\boldsymbol{\alpha}^*(\mathbf{X}_{il}, \mathbf{X}_i) = \{\alpha_k^*(\mathbf{X}_{il}, \mathbf{X}_i), k = 1, \dots, p\}^\top$. We can estimate $g^*, \boldsymbol{\alpha}^*$ by minimizing the negative log-likelihood

$$\begin{aligned} \mathcal{L}(g, \boldsymbol{\alpha}) &= -n^{-1} \sum_{i=1}^n (Y_i g\{\mathbf{S}_i(\boldsymbol{\alpha})\} - h[g\{\mathbf{S}_i(\boldsymbol{\alpha})\}]) \text{ subject to} \\ g &\in \mathcal{F}_g, \omega_k \in \mathcal{F}_{\omega_k}, \alpha_k(\mathbf{X}_{il}, \mathbf{X}_i) = \exp\{\omega_k(\mathbf{X}_{il})\} / \sum_{l=1}^d \exp\{\omega_k(\mathbf{X}_{il})\}, \\ \boldsymbol{\alpha}(\mathbf{X}_{il}, \mathbf{X}_i) &= \{\alpha_k(\mathbf{X}_{il}, \mathbf{X}_i), k = 1, \dots, p\}^\top \end{aligned} \quad (4)$$

where $h(x) = \log\{1 + \exp(x)\}$. Let $\hat{g}, \hat{\boldsymbol{\alpha}}$ be the resulting estimators.

In practice, we employ the network architecture depicted in Figure 2 to approximate the true functions $g^*, \boldsymbol{\alpha}^*$. As shown in Figure 2, the core structure consists of a series of recursive CNN layers followed by a fully connected layer. We use Blocks 1 and 2 to construct functions in \mathcal{F}_{ω_k} , $k = 1, \dots, p$, which approximate $\boldsymbol{\alpha}^*$. The resulting function is then fed into Blocks 3 and 4 to build a function in \mathcal{F}_g that approximates g^* .

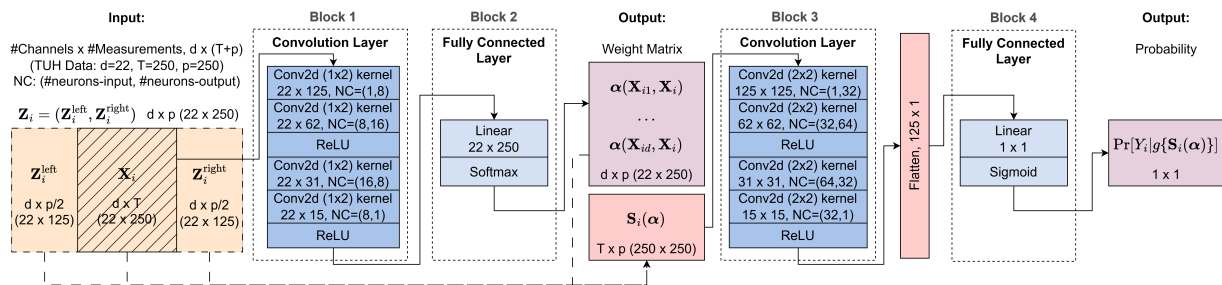


Figure 2: The deep neural network diagram to approximate the true functions $g^*, \boldsymbol{\alpha}^*$.

4 Real Data Analysis

We apply NDL on three real datasets, including a public scalp EEG dataset from TUH, a private MEG dataset from UCSF, and a private EEG dataset from BTH. We also compare NDL with two existing methods, the SpikeDet adopting template matching (Nonclercq and Ercek 2016) and a deep learning method in Munia et al. (2023) using the TUH data.

4.1 Data and preprocessing

4.1.1 The **TUH** dataset (Harati et al. 2015) is the only publicly available scalp interictal EEG dataset that includes per-channel annotations. The dataset consists of 511 continuous EEG recordings using the standard 10/20 channel configuration, collected from 370 patients. Each recording is collected at a sampling frequency of 250 Hz. We filter the data and retain frequencies between 1 and 45 Hz to remove the slow wave and fast oscillation caused by the artifacts and noise. Then we remove the linear trend of the data. The data are then transformed into the Temporal Central Parasagittal montage, as described in Lopez et al. (2016), using the 22 channels listed in Table S1 in the supplementary material. This montage was chosen because it has been used when labeling the data.

Each recording has one or more one-second annotations on these 22 channels. According to Obeid and Picone (2016), these annotations include six classes: (1) spike and sharp wave (SPSW), (2) generalized periodic epileptiform discharge (GPED), (3) periodic lateralized epileptiform discharge (PLED), (4) eye movement (EYEM), (5) artifact (ARTF), and (6) background (BCKG). Among the six classes, SPSW, GPED and PLED are abnormal events of clinical interest, while EYEM, ARTF and BCKG are artifacts and normal signals.

We extract a two-second segment around each annotation, where the middle one-second segment is treated as \mathbf{X}_i and the remaining forms \mathbf{Z}_i . Both \mathbf{X}_i and \mathbf{Z}_i are 22×250 . Figure 3 provides examples of the two-second segments for each class of the annotations. Table 1 reports the number of segments and the number of patients for each class.

4.1.2 The **USCF MEG** data are recorded from 277 epilepsy patients who have undergone MEG tests at the MEG center of UCSF between 2019 and 2022. Each MEG recording has a labeling file stored on the clinical server. First, the recording is fully screened by a

Table 1: TUH: Numbers of segments and corresponding numbers of patients for each of the six classes, in both the training set and the testing set.

TUH Data		Abnormal			Normal		
		SPSW	GPED	PLED	EYEM	ARTF	BCKG
Training	# Segments	139	2404	1890	520	1624	3195
	# Patients	27	30	29	41	134	200
Testing	# Segments	46	819	700	124	519	1187
	# Patients	9	21	20	34	41	74

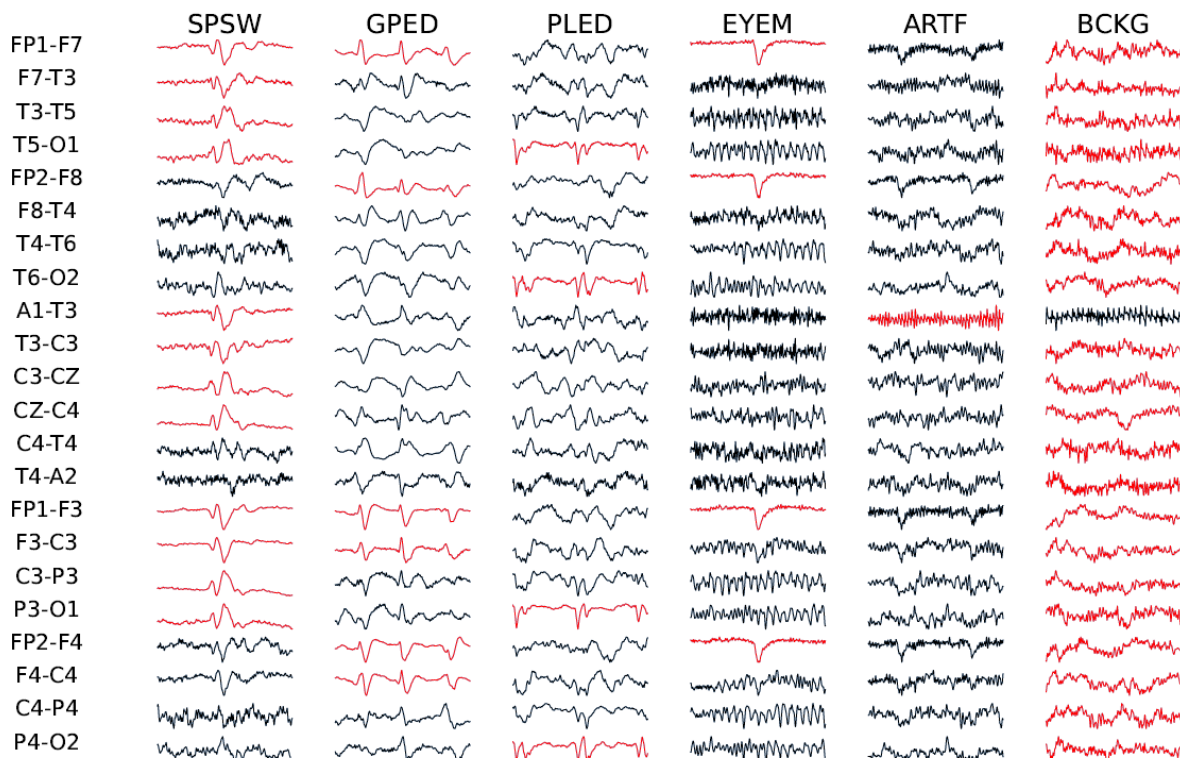


Figure 3: TUH: Two-second segments of the six classes of events with 22 ACNS TCP montages, where the annotated channels are shown in red.

technologist to mark out candidate spikes. These candidate spikes are then reviewed by a clinician, often with 1 or 2 residents, to confirm the presence of the spikes. This process ensures that the spike labels are validated through multiple readers.

The recordings are collected at a sampling frequency of 600 Hz on 140 channels. We filter the data to retain frequencies between 1 and 45 Hz, downsample the data to 256 Hz, and remove the linear trend of the data. Since the spike labels are less than 250 milliseconds, we extract a segment of 0.5 seconds around each label, where the middle 0.25-second segment is treated as \mathbf{X}_i and the remaining is combined as \mathbf{Z}_i . Both \mathbf{X}_i and \mathbf{Z}_i are 140×64 . We also extract 0.5-second background segments from non-spike labeled time. These background segments can accurately represent non-spike activities. We obtain 230,325 segments, among which 46% are spike segments labeled in the clinical notes.

4.1.3 This **BTH EEG** dataset is collected at China’s Beijing Tiantan Hospital, to test the adaptability of NDL across multi-modal data. The dataset consists of 142 EEG segments with 19 channels from 20 patients, with 53 segments containing spike signals. The raw data are collected at a sampling frequency of 512 Hz. We apply a filter to retain frequencies between 1 and 45 Hz, downsample the data to 256 Hz, and remove the linear trend of the data. The data are then converted into the common average montage. The spikes are labeled and confirmed by two trained clinicians. We extract 0.5-second time segments around the labeled spikes and normal background activities, where the middle 0.25-second segment is treated as \mathbf{X}_i and the remaining forms \mathbf{Z}_i . Both \mathbf{X}_i and \mathbf{Z}_i are 19×64 . Finally, we apply the pre-trained model from the UCSF MEG data on the out-of-sample EEG data, to evaluate NDL’s adaptability across different datasets.

4.2 Results from the TUH Data

We apply NDL to the binary classification of normal and abnormal segments. Let TP , TN , FP , and FN represent true positive, true negative, false positive, and false negative, respectively. We then report the following metrics evaluated on the testing data:

1. Sensitivity $:= TP/(TP + FN)$
2. Precision $:= TP/(TP + FP)$
3. Specificity $:= TN/(TN + FP)$
4. F1 score $:= TP/(TP + \frac{1}{2}(FP + FN))$
5. PRAUC: The area under the precision-recall curve
6. AUC: The area under the receiver operating characteristic (ROC) curve.

We further divide the training data into two groups: 80% of the training samples are used to estimate the parameters; 20% of the samples are used to validate the tuning parameter choices. As shown in Figure 4 (a), the training loss and the validation loss decrease rapidly in the first 10 epochs and become stable after the 40th epoch. Meanwhile, as shown in Figure 4 (b), the AUC and PRAUC of the validation set stay above and near 90%, respectively, after around 10 epochs. Sensitivity, precision, and F1 score all stay above 80% after around 40 epochs with the threshold set as 0.5.

Figures 4 (c) and (d) present the ROC curve and the precision-recall curve. The AUC and PRAUC on the testing data are 93.53% and 92.66%, respectively, illustrating high accuracy and precision of the proposed method. In Table 2, we then compare NDL with SpikeDet (Nonclercq and Ercek 2016), an open-source spike detection algorithm of Nonclercq et al. (2009), and the deep learning method of Munia et al. (2023). The comparison

is evaluated using the same testing set of the TUH data. As one can see, NDL outperforms the other methods for all the measures (boldface). Since the output of SpikeDet is binary and the specificity, PRAUC and AUC for the method proposed by Munia et al. (2023) are not reported, we do not provide the PRAUC and AUC values for the two methods.

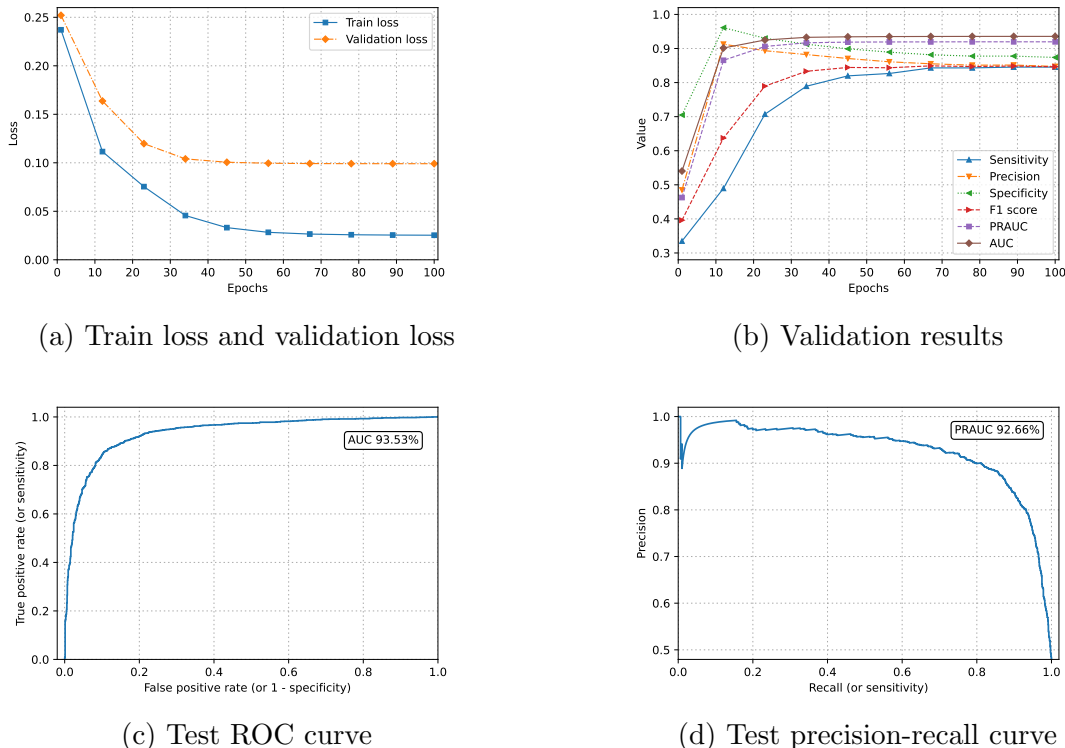


Figure 4: TUH: Results from NDL with fine-tuned hyperparameters.

In addition to binary classification, we can estimate the p -dimensional weight $\hat{\alpha}(\mathbf{X}_{il}, \mathbf{X}_i)$ for each channel. By summing the p entries of the weight $\hat{\alpha}(\mathbf{X}_{il}, \mathbf{X}_i)$, we determine the importance of Channel l as $\mathbf{1}^\top \hat{\alpha}(\mathbf{X}_{il}, \mathbf{X}_i)$. By ranking this importance from highest to lowest, we can select the top L channels as the ones that are most likely to contain spikes.

To assess this approach, we cross-check the selected top channels with the actual channel labels from the TUH data to check whether our model can identify spike-containing channels better than random selection. Figure 5 illustrates the probability that the top L channels of a segment contain a true spike, comparing NDL ranking with random ranking based on

Table 2: TUH: Comparison of NDL, SpikeDet and the method of Munia et al. (2023). AUC and PRAUC are unavailable in SpikeDet and are not reported in Munia et al. (2023).

TUH Data	Sensitivity	Precision	Specificity	F1 score	PRAUC	AUC
NDL	0.87	0.87	0.88	0.87	0.93	0.94
SpikeDet	0.50	0.74	0.83	0.59	-	-
Munia et al. (2023)	0.75	0.73	-	0.74	-	-

the testing data. We create the 95% confidence interval of the probability through resample procedures with different initial values generated from different random seeds. It is obvious that NDL performs much better in identifying those channels with spikes. Furthermore, NDL ignores background channels (last pair of side-by-side boxplots).

4.3 Results from the UCSF MEG Data

We use 95% of the data for training and the remaining 5% for testing. Table 3 summarizes the excellent performance on the testing data, for example, an AUC of 91.61%.

Table 3: UCSF MEG: Testing Results.

UCSF MEG Data	Sensitivity	Precision	Specificity	F1 score	PRAUC	AUC
NDL	0.77	0.84	0.91	0.81	0.87	0.92

We visualize the distribution of the most important channels using topographical graphs and barplots, where the topographical graph is a 2D representation of the probabilities of being the top L channels identified by NDL ranking. Figure 6 contains six topographical graphs, illustrating the probabilities of being identified as one of the most important L channels out of the 140 MEG channels based on the training set and the testing set,

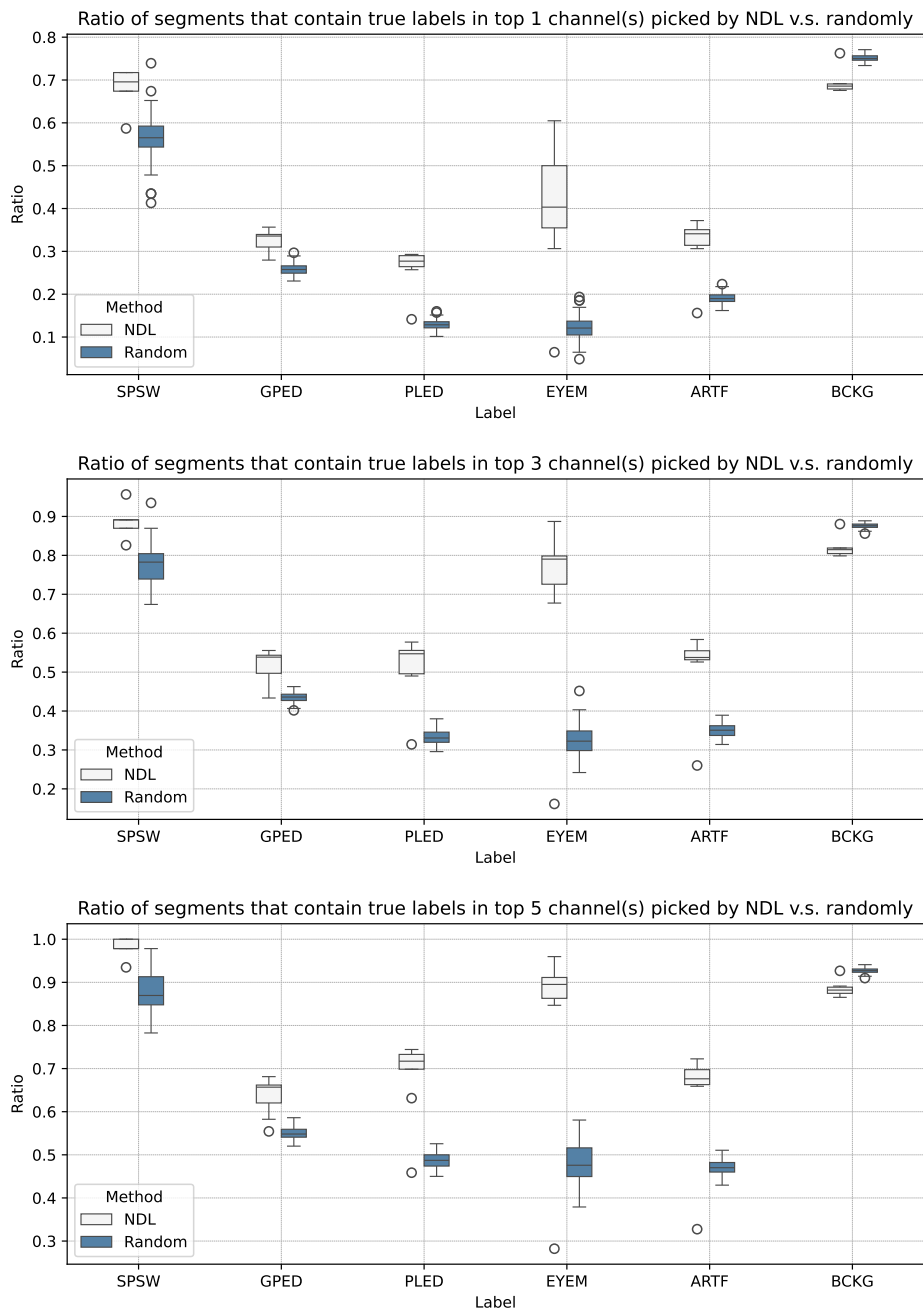


Figure 5: TUH: Side-by-side boxplots comparing the top channels selected by NDL ranking with random ranking through 100 repetitions.

respectively. Figure 7 shows the distribution of the top L channels across different brain lobes. Figures 6 and 7 both indicate that the spikes often occur in the temporal lobes. This is consistent with the clinical finding that seizures usually happen in the temporal lobes (McIntosh and Das 2019).

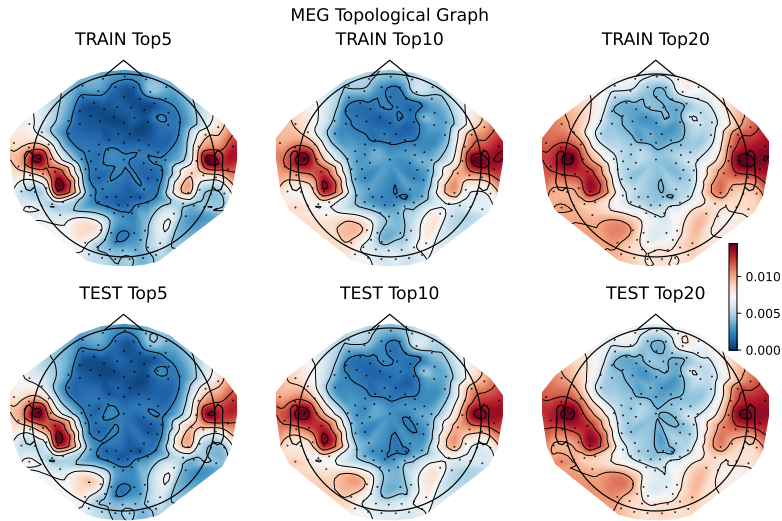


Figure 6: UCSF MEG: The topological distributions of the probabilities of being the top channels identified by NDL ranking.

4.4 Results from the BTH EEG Data

We take the model trained on the UCSF MEG data and test it on the BTH EEG data. This analysis aims to evaluate the adaptability of NDL across different modalities with varying channels. Even without retraining, NDL achieves an AUC of 84.18% and a sensitivity of 94.34%. The results show that NDL adapts well in out-of-sample cross-modality scenarios.

We present three topographical graphs in Figure 8 showing the probability of each channel being selected as one of the top L channels by NDL. Furthermore, Figure 9 shows the distribution of the top L channels in different lobes. Interestingly, in addition to the temporal lobes, the pre-frontal regions are also frequently selected. Our neurology

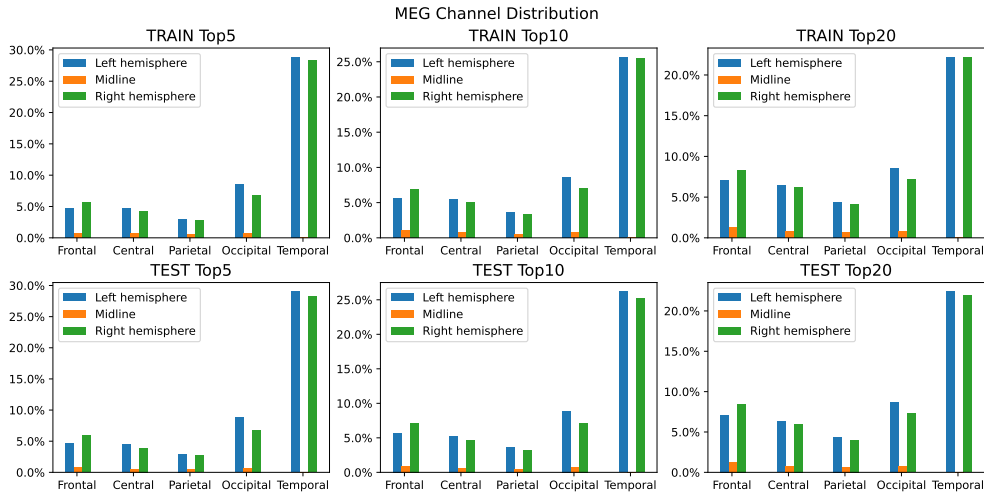


Figure 7: UCSF MEG: Histograms of the distributions of the top channels identified by NDL ranking, on five different lobes.

collaborators confirm that this is not unexpected, as scalp EEG spikes can often be confused with eye movements, which typically occur in the pre-frontal areas. More data are needed to fine-tune the model for better adaptation to the EEG data.

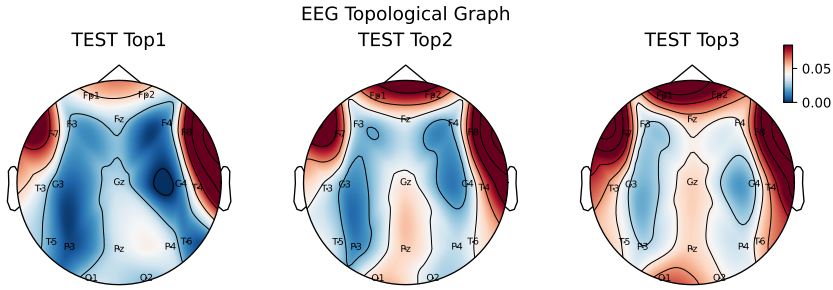


Figure 8: BTH EEG: The topological distributions of the probabilities of being selected into the top channels NDL ranking.

4.5 Procedures to adopt to continuous time series data

Unlike the segmented data analyzed in the previous subsections, neurophysiology data are usually recorded continuously in real-world settings. We develop the following Algorithm 1 that applies NDL to continuous time series data in practice.

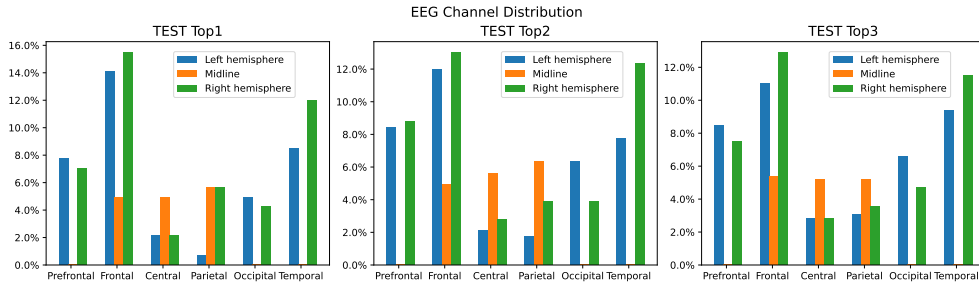


Figure 9: BTH EEG: Histograms of the distributions of the top channels selected by NDL ranking, on six different lobes.

Algorithm 1 employs a sliding window technique to extract overlapping data segments and evaluate the probability of containing a spike for each segment. We then identify those time segments where the probability exceeds a specified threshold C as initial candidates. Finally, we apply a non-maximum suppression algorithm to eliminate overlapping candidates, resulting in the final set of confirmed segments.

We apply Algorithm 1 to the testing set of the UCSF MEG data and to the BTH EEG Data. Figure 10(a) presents the results of applying NDL to a continuous MEG recording from UCSF. The detection S1 accurately identifies the true spikes in the right temporal lobe, followed by an additional detection S2 shortly afterward. Although S2 appears outside the 0.25-second window according to the true spike labels, the detection remains valid since the true labels mark the onset of the spikes, and spikes may propagate to other channels over time. Moreover, our detection effectively highlights the channels where spikes occur, showing its accuracy in identifying spike-related activity across multiple channels.

Figure 10(b) shows the results of applying NDL to the continuous EEG data from BTH. The detection S3 accurately identifies a true spike on the F7-avg channel. The detections S4 and S5 capture eye movements on the Fp1-avg and Fp2-avg channels, respectively. Eye movement artifacts typically appear simultaneously on these two channels since they are closest to the eyes. In practice, if both channels are identified as important, it is likely

that the detection relates to eye movements rather than true spikes. Identification of key channels plays a crucial role in reducing false positives by helping to distinguish between eye movement artifacts and genuine spike activities.

Algorithm 1 The sliding window algorithm

Input: Preprocessed MEG and EEG recordings with d channels and a total of T_0 time measurements; a segmentation time length T ; a cutoff C .

- 1: **for** $t = T/2, \dots, T_0 - T/2$ **do**
 - 2: Set the window between the $(t - T/2 + 1)$ th and the $(t + T/2)$ th time points.
 - 3: Estimate the probability $\hat{g}_{(t)}$ and the weight $\hat{\alpha}_{(l,t)}$ for Channel l .
 - 4: **if** $\hat{g}_{(t)} > C$ and $\mathbf{1}^\top \hat{\alpha}_{(l,t)} > (1.5/d)(\sum_{l=1}^d \mathbf{1}^\top \hat{\alpha}_{(l,t)})$ **then**
 - 5: Select the segment between the window as a candidate.
 - 6: **end if**
 - 7: Remove duplicates by clustering the candidate segments based on time, utilizing the Density-Based Spatial Clustering of Applications with Noise (DBSCAN) method (Ester et al. 1996).
 - 8: Select the segment with the highest spike probability within each cluster as the final representation.
 - 9: **end for**
-

5 Simulation

We evaluate NDL using simulation studies with different sample sizes n to examine the convergence of the estimation procedure.

To simulate data that closely resemble real-world conditions, we randomly segment $d \times (T + p)$ brain signal matrices from the TUH data, with $d = 22$, $T = 64$ and $p = 64$. Each

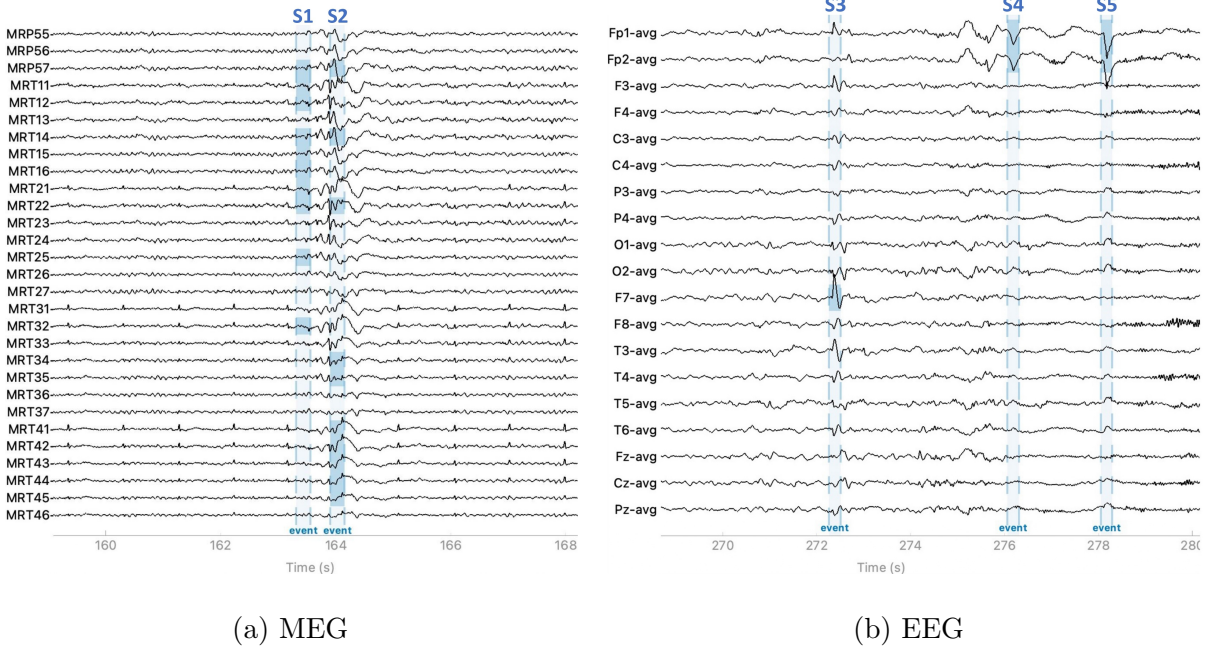


Figure 10: MEG and EEG recordings annotated by NDL using Algorithm 1, with top channels highlighted in a dark color for each detection.

matrix is standardized by subtracting the mean of its rows and dividing by the standard deviation of its elements. We then extract the segment between the $(p/2 + 1)$ th column and the $(p/2 + T)$ th column as \mathbf{X}_i , forming a $d \times T$ matrix. The remaining columns are used as \mathbf{Z}_i , a $d \times p$ matrix. We choose the true functions $\omega_k^*(\mathbf{X}_{il})$, $k = 1, \dots, p$, randomly with replacement from the following set:

$$\left\{ \log \left(\sum_{t=1}^T (X_{ilt})^2 / T - \mu_{il}^2 \right), -\log \left(\sum_{t=1}^T (X_{ilt})^2 / T - \mu_{il}^2 \right), \right. \\ \left. \left(\sum_{t=1}^T (z_{ilt})^3 / T \right), -\left(\sum_{t=1}^T (z_{ilt})^3 / T \right), \left(\sum_{t=1}^T (z_{ilt})^4 / T - 3 \right), -\left(\sum_{t=1}^T (z_{ilt})^4 / T - 3 \right), \right. \\ \left. \log \left(\sum_{t=1}^T |X_{ilt} \sin(X_{ilt})| \right), \log \left(\sum_{t=1}^T |X_{ilt} \cos(X_{ilt})| \right) \right\},$$

where $z_{ilt} = (X_{ilt} - \mu_{il}) / \sigma_{il}$ with $\mu_{il} = \sum_{t=1}^T X_{ilt} / T$ and $\sigma_{il} = \sqrt{\sum_{t=1}^T (X_{ilt})^2 / T - \mu_{il}^2}$. Furthermore, we generate $\boldsymbol{\beta}_1 = (\beta_{11}, \dots, \beta_{1T})^\top$ and $\boldsymbol{\beta}_2 = (\beta_{21}, \dots, \beta_{2p})^\top$ from the standard multivariate normal distributions and β_0 from the standard normal distribution. The coefficient parameters $\{\beta_0, \boldsymbol{\beta}_1, \boldsymbol{\beta}_2\}$ are fixed for all simulation repetitions. Finally, we define

$g^* \{\mathbf{S}_i(\boldsymbol{\alpha}^*)\} = \boldsymbol{\beta}_1^\top \mathbf{S}_i(\boldsymbol{\alpha}^*) \boldsymbol{\beta}_2 + \beta_0$, and sample Y_i as a Bernoulli variable with the probability of success being $(\exp[-g^* \{\mathbf{S}_i(\boldsymbol{\alpha}^*)\}] + 1)^{-1}$.

We apply NDL to each simulated sample set $\{(\mathbf{X}_i, \mathbf{Z}_i, Y_i), i = 1, \dots, n\}$ and obtain the resulting estimators $\hat{\boldsymbol{\alpha}}, \hat{g}$. Then we measure the estimation errors of $\hat{\boldsymbol{\alpha}}$ and \hat{g} , respectively:

$$d_{\boldsymbol{\alpha}^*}(\hat{\boldsymbol{\alpha}}) = \frac{1}{N} \sum_{i=1}^N \|\{\hat{\boldsymbol{\alpha}}(\mathbf{X}_{il}, \mathbf{X}_i), l = 1, \dots, d\}^\top - \{\boldsymbol{\alpha}^*(\mathbf{X}_{il}, \mathbf{X}_i), l = 1, \dots, d\}^\top\|_2,$$

and

$$d_{g^*}(\hat{g}) = \frac{1}{N} \sum_{i=1}^N |h'[\hat{g}\{\mathbf{S}_i(\hat{\boldsymbol{\alpha}})\}] - h'[g^*\{\mathbf{S}_i(\hat{\boldsymbol{\alpha}})\}]|,$$

where $N = 4096$ samples are randomly selected from simulated data to evaluate the estimation errors of the functions.

We generate data for five settings of varying sample sizes $n_j = 2^{10+j}$, $j = 1, \dots, 5$. Each setting is repeated 10 times. Figure 11 shows that $d_{\boldsymbol{\alpha}^*}(\hat{\boldsymbol{\alpha}})$ and $d_{g^*}(\hat{g})$ decrease as the sample size n increases. One can see that both $\boldsymbol{\alpha}(\mathbf{X}_{il}, \mathbf{X}_i)$ and $g\{\mathbf{S}_i(\boldsymbol{\alpha})\}$ are identifiable and our estimators converge to the true values as the sample size increases.

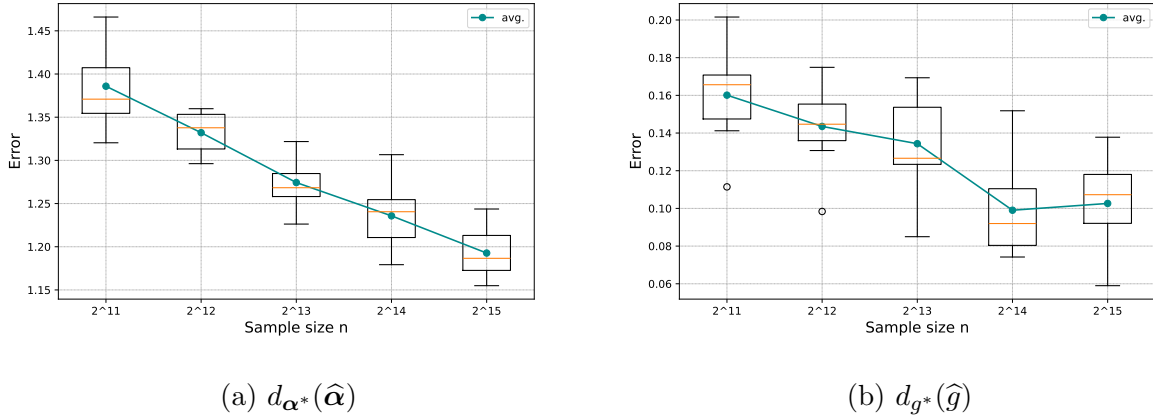


Figure 11: Boxplots of the estimation errors under different sample sizes over 10 repetitions.

6 Theoretical Results

We derive the convergence rate and establish the asymptotic consistency of the estimators.

6.1 Necessary definitions and conditions

Below we first present some necessary definitions and conditions. Let $g_0 \in \mathcal{F}_g, \omega_{0k} \in \mathcal{F}_{\omega_k}, k = 1, \dots, T$ such that $g_0 \equiv \operatorname{argmin}_{g \in \mathcal{F}_g} \|g - g^*\|_\infty$, and $\omega_{0k} \equiv \operatorname{argmin}_{\omega_k \in \mathcal{F}_{\omega_k}} \|\omega_k - \omega_k^*\|_\infty$. where g^*, ω_k^* are the true functions in $\mathcal{G}_g, \mathcal{G}_{\omega_k}$, respectively. Let $\alpha_{0k}(\mathbf{X}_{il}, \mathbf{X}_i) = \exp\{\omega_{0k}(\mathbf{X}_{il})\} / \sum_{l=1}^d \exp\{\omega_{0k}(\mathbf{X}_{il})\}$ and $\boldsymbol{\alpha}_0 = \{\alpha_{0k}, k = 1, \dots, p\}^\top$. Here, g_0 and ω_{0k} represent the functions within the neural network spaces \mathcal{F}_g and \mathcal{F}_{ω_k} that are closest to g^* and ω_k^* , respectively. Let $\psi_g = g - g_0$ and $\psi_{\alpha_k} = \alpha_k - \alpha_{0k}$ for arbitrary functions $g \in \mathcal{F}_g$ and $\alpha_k \in \mathcal{H}_{\alpha_k}$, where

$$\mathcal{H}_k \equiv \left\{ \alpha_k = \exp\{\omega_k(\mathbf{X}_{il})\} / \sum_{l=1}^d \exp\{\omega_k(\mathbf{X}_{il})\} : \omega_k \in \mathcal{F}_{\omega_k}, k = 1, \dots, p \right\}.$$

Let $\boldsymbol{\psi}_\alpha = \{\psi_{\alpha_k}, k = 1, \dots, p\}^\top$. Furthermore, let $\boldsymbol{\alpha}^{(-k)} = (\alpha_1, \dots, \alpha_{k-1}, \alpha_{k+1}, \dots, \alpha_p)$ and

$$\begin{aligned} & \Omega(g_0, \boldsymbol{\alpha}_0, \psi_g, \boldsymbol{\psi}_\alpha, \epsilon_g^\dagger, \boldsymbol{\epsilon}_\alpha^\dagger) \\ &= \left\{ \frac{\partial^2 \mathcal{L}(g_0 + \epsilon_g \psi_g, \boldsymbol{\alpha})}{\partial \epsilon_g^2} + 2 \sum_{k=1}^p \frac{\partial^2 \mathcal{L}(g_0 + \epsilon_g \psi_g, \alpha_{0k} + \epsilon_{\alpha_k} \psi_{\alpha_k}, \boldsymbol{\alpha}^{(-k)})}{\partial \epsilon_g \partial \epsilon_{\alpha_k}} \right. \\ & \quad \left. + \sum_{k=1}^p \sum_{j=1}^p \frac{\partial^2 \mathcal{L}(g_0, \alpha_{01}, \dots, \alpha_{0l} + \epsilon_{\alpha_l} \psi_{\alpha_l}, \dots, \alpha_{0u} + \epsilon_{\alpha_u} \psi_{\alpha_u}, \dots, \alpha_{0p})}{\partial \epsilon_{\alpha_j} \partial \epsilon_{\alpha_u}} \right\} \Big|_{\epsilon_g = \epsilon_g^\dagger, \epsilon_{\alpha_k} = \epsilon_{\alpha_k}^\dagger, k=1, \dots, p}, \end{aligned}$$

where $\epsilon_g^\dagger, \epsilon_{\alpha_k}^\dagger \in (0, 1), k = 1, \dots, p$ and $\boldsymbol{\epsilon}_\alpha^\dagger = (\epsilon_{\alpha_k}^\dagger, k = 1, \dots, p)^\top$. Define the rates

$$\phi_{\omega_j n} \equiv \max_{i=0, \dots, q_{\omega_j}} n^{-\frac{2\beta_{\omega_j}^* i}{2\beta_{\omega_j}^* i + t_{\omega_j} i}}, \phi_{g n} \equiv \max_{i=0, \dots, q_g} n^{-\frac{2\beta_{g_i}^*}{2\beta_{g_i}^* + t_{g_i}}}, \quad (5)$$

where $\beta_{\omega_j}^* \equiv \beta_{\omega_j} \prod_{l=i+1}^{q_{\omega_j}} \{\min(\beta_{\omega_{jl}}, 1)\}$ and $\beta_{g_i}^* \equiv \beta_{g_i} \prod_{l=i+1}^{q_g} \{\min(\beta_{gl}, 1)\}$.

Now we present the necessary conditions to guarantee the convergence of the estimators.

(C1) Assume $F_{\omega_j} \geq \max(K_{\omega_j}, 1), j = 1, \dots, p$ and $F_g \geq \max(K_g, 1)$.

(C2) Assume $\sum_{i=0}^{q_{\omega_j}} \log_2 \{\max(4t_{\omega_j i}, 4\beta_{\omega_j i})\} \log_2 n \leq L_{\omega_j} \lesssim n\phi_{\omega_j n}, j = 1, \dots, p$,
and $\sum_{i=0}^{q_g} \log_2 \{\max(4t_{gi}, 4\beta_{gi})\} \log_2 n \leq L_g \lesssim n\phi_{gn}$.

(C3) Assume $n\phi_{\omega_j n} \lesssim \min_{u=1, \dots, L} p_{\omega_j u}, j = 1, \dots, p$ and $n\phi_{gn} \lesssim \min_{u=1, \dots, L_g} p_{gu}$.

(C4) Assume $s_{\omega_j} \asymp n\phi_{\omega_j n} \log n, j = 1, \dots, p$ and $s_g \asymp n\phi_{gn} \log n$. And assume $(s_g/L_g)^{L_g/2} \leq M_L < \infty$.

(C5) Assume $X_{ilt}, Z_{ilj} \in [-\max(K_{\omega_j}, K_g, j = 1, \dots, p), \max(K_{\omega_j}, K_g, j = 1, \dots, p)] \subseteq [-C_M, C_M]$.

(C6) Assume $c_\psi < h''(\cdot) < C_\psi$ and $0 < |h'''(\cdot)| < \infty$, and $Y_i - h'[g^* \{\mathbf{S}_i(\boldsymbol{\alpha}^*)\}]$ is a mean zero sub-Gaussian random variable.

(C7) Assume that

$$\begin{aligned} & 0 < \alpha_{\min} E \left[\psi_g \{\mathbf{S}_i(\boldsymbol{\alpha}_0)\}^2 + \sum_{j=1}^p \sum_{l=1}^d T\psi_{\alpha_j}(\mathbf{X}_{il}, \mathbf{X}_i)^2 \right] \\ & \leq \inf_{\epsilon_g, \epsilon_\alpha} E\{\Omega(g_0, \boldsymbol{\alpha}_0, \psi_g, \boldsymbol{\psi}_\alpha, \epsilon_g, \boldsymbol{\epsilon}_\alpha)\} \leq \sup_{\epsilon_g, \epsilon_\alpha} E\{\Omega(g_0, \boldsymbol{\alpha}_0, \psi_g, \boldsymbol{\psi}_\alpha, \epsilon_g, \boldsymbol{\epsilon}_\alpha)\} \\ & \leq \alpha_{\max} E \left[\psi_g \{\mathbf{S}_i(\boldsymbol{\alpha}_0)\}^2 + \sum_{j=1}^p \sum_{l=1}^d T\psi_{\alpha_j}(\mathbf{X}_{il}, \mathbf{X}_i)^2 \right] < \infty. \end{aligned}$$

Conditions (C1)–(C4) are standard assumptions to ensure that a deep learning network can approximate the true function with an error that vanishes as the sample size increases, as shown in Lemma S2 in the supplementary materials. Condition (C5) requires bounded predictors, which are easily met in real data. Conditions (C6)–(C7) are commonly assumed to ensure estimation consistency under the generalized linear model.

6.2 Theoretical properties

Lemma 1 *Assuming Conditions (C1) –(C6) hold, and $T, p \leq s_g$, there are positive constants $C_g, C_{\omega_j}, c_g, c_{\omega_j}$ such that, with probability one,*

$$|h' [g^* \{\mathbf{S}_i(\boldsymbol{\alpha}^*)\}] - h' [g_0 \{\mathbf{S}_i(\boldsymbol{\alpha}_0)\}]| \leq \left\{ C_g \max_{u=0, \dots, q_g} c_g^{-\frac{\beta_{gu}^*}{t_{gu}}} n^{-\frac{\beta_{gu}^*}{2\beta_{gu}^* + t_{gu}}} + 2C_M M_L \sqrt{d \min(s_g, Tp)} \sup_{j=1, \dots, p} C_{\omega_j} \max_{u=0, \dots, q_{\omega_j}} c_{\omega_j}^{-\frac{\beta_{\omega_j u}^*}{t_{\omega_j u}}} n^{-\frac{\beta_{\omega_j u}^*}{2\beta_{\omega_j u}^* + t_{\omega_j u}}} \right\}.$$

The proof of Lemma 1 is presented in Section S4 in the supplementary material. Note that $h'(\cdot)$ is the expit function: $h' [g^* \{\mathbf{S}_i(\boldsymbol{\alpha}^*)\}]$ represents the true probability of $Y_i = 1$. Lemma 1 shows that the distance between the deep learning approximation of the success probability and the truth depends on how well g_0 and $\boldsymbol{\alpha}_0$ approximate the true values. This distance decreases at the standard nonparametric rate as the sample size grows.

For the positive constants $C_0, A_g, A_{\omega_j}, a_g, a_{\omega_j}, j = 1, \dots, p$, we define

$$\eta(A_g, a_g, \mathbf{A}_\omega, \mathbf{a}_\omega) \equiv \sqrt{C_0 \log(n)/(cn)} + \left\{ A_g \max_{u=0, \dots, q_g} a_g^{-\frac{\beta_{gu}^*}{t_{gu}}} n^{-\frac{\beta_{gu}^*}{2\beta_{gu}^* + t_{gu}}} + 2C_M M_L \sqrt{d \min(s_g, Tp)} \sup_{j=1, \dots, p} A_{\omega_j} \max_{u=0, \dots, q_{\omega_j}} a_{\omega_j}^{-\frac{\beta_{\omega_j u}^*}{t_{\omega_j u}}} n^{-\frac{\beta_{\omega_j u}^*}{2\beta_{\omega_j u}^* + t_{\omega_j u}}} \right\},$$

where $\mathbf{A}_\omega = (A_{\omega_j}, j = 1, \dots, p)^\top$, and $\mathbf{a}_\omega = (a_{\omega_j}, j = 1, \dots, p)^\top$.

Theorem 1 *Let $\psi_{\hat{g}} = \hat{g} - g_0$ and $\psi_{\hat{\alpha}_j} = \hat{\alpha}_j - \alpha_{0j}$. Assume $\hat{\alpha}_j, \alpha_{0j} \in \mathcal{H}_j$, $\omega_j^* \in \mathcal{G}_{\omega_j}$, $\hat{g}, g_0 \in \mathcal{F}_g$, and $g^* \in \mathcal{G}_g$. Assume $T, p < s_g$ and Conditions (C1)–(C7) hold. Let $dP_{\boldsymbol{\alpha}}(\cdot)$ be the probability density function of $\mathbf{S}_i(\boldsymbol{\alpha})$, and assume $\|dP_{\boldsymbol{\alpha}_0}(\mathbf{z})/dP_{\boldsymbol{\alpha}^*}(\mathbf{z})\|_\infty \geq m_h > 0$. Furthermore, let $dP_{\mathbf{X}}(\cdot)$ be the probability density for \mathbf{X}_i . Then there are positive constants*

$D_g, d_g, \mathbf{D}_\omega = (D_{\omega_j}), \mathbf{d}_\omega = (d_{\omega_j}), D_{g1}, d_{g1}, D_{\omega_j1}, d_{\omega_j1}, c'_H, C_H$ such that

$$\begin{aligned} & \int \{\widehat{g}(\mathbf{z}) - g^*(\mathbf{z})\}^2 dP_{\alpha^*}(\mathbf{z}) + \sum_{j=1}^p \int \sum_{l=1}^d \{\widehat{\alpha}_j(\mathbf{x}_l, \mathbf{x}) - \alpha_j^*(\mathbf{x}_l, \mathbf{x})\}^2 dP_{\mathbf{X}}(\mathbf{x}) \\ & \leq 16 \min(m_h, 1)^{-1} \alpha_{\min}^{-1} \left(C_M M_L \eta(D_g, d_g, \mathbf{D}_\omega, \mathbf{d}_\omega) \left[\min(s_g, Tp)^{1/2} \{\log(n)/(cn)\}^{1/4} \right. \right. \\ & \quad \left. \left. + \{\log(n)/(cn)\}^{1/4} \right] + TpC_1 \log^2(n) \left\{ \phi_{gn} L_g + \sum_{j=1}^p \phi_{\omega_j n} L_{\omega_j} \right\} + C_H Tp/n \right) \\ & \quad + 32 \min(m_h, 1)^{-1} C_M M_L dp \alpha_{\min}^{-2} \eta(D_g, d_g, \mathbf{D}_\omega, \mathbf{d}_\omega)^2 + \left(D_{g1} \phi_{gn} + T \sum_{j=1}^p D_{\omega_j1} \phi_{\omega_j n} \right) \end{aligned}$$

with probability greater than $1 - 6n^{-1} - 2 \exp \left[-nC_1 \log^2(n) \left\{ \phi_{gn} L_g + \sum_{j=1}^p \phi_{\omega_j n} L_{\omega_j} \right\} \right]$.

When $n \rightarrow \infty$ and T, p are finite, we have

$$\int \{\widehat{g}(\mathbf{z}) - g^*(\mathbf{z})\}^2 dP_{\alpha^*}(\mathbf{z}) + \sum_{j=1}^p \int \sum_{l=1}^d \{\widehat{\alpha}_j(\mathbf{x}_l, \mathbf{x}) - \alpha_j^*(\mathbf{x}_l, \mathbf{x})\}^2 dP_{\mathbf{X}}(\mathbf{x}) \xrightarrow{p} 0.$$

The upper bound of the error is dominated by $TpC_1 \log^2(n) \left\{ \phi_{gn} L_g + \sum_{j=1}^p \phi_{\omega_j n} L_{\omega_j} \right\}$ when T and p are finite. Also because ϕ_{gn} and $\phi_{\omega_j n}$ are of the order of the inverse of polynomial functions of n , the upper bound approaches zero with the probability increasing to one as the sample size $n \rightarrow \infty$. This shows that the error converges to zero in probability.

The proof of the theorem is presented in Section S6 in the supplementary material. To prove the theorem, Lemma S6 shows that the first derivative of the objective function has an upper bound that approaches zero as the sample size increases; Lemma S7 then shows that the second derivative is asymptotically a positive definite matrix. We then derive the final results by combining these findings with the convergence of the deep learning function presented in Lemma 1.

7 Conclusion and Discussion

We have developed the NDL method as an interpretable alternative to traditional deep learning methods for spike detection. This method can adapt to different channel types,

making it a foundational model for neurophysiological data analysis. We have established the model’s identifiability and demonstrated the asymptotic consistency of its estimation procedure. NDL has been applied to the publicly available TUH data, the private UCSF MEG data, and the private BTH EEG data. Our analyses show that NDL outperforms existing methods in terms of sensitivity and specificity in spike detection. Moreover, it effectively identifies channels containing relevant events. Finally, we demonstrate that a model trained on the UCSF MEG data can be successfully applied to the BTH EEG data, highlighting NDL’s capacity to integrate multiple datasets and serve as a foundation model that can be fine-tuned for different targets.

In this paper, our model is trained on the TUH data from 370 subjects and the UCSF MEG data from 277 subjects. Due to the limited sample sizes, the model may not fully capture the variation in spike waveforms across different populations. We are currently collaborating with clinicians to label more EEG and MEG data to improve the model’s accuracy across a broader range of populations. The tools developed in this paper will be used as a screening process to identify spike candidates, streamlining the labeling process in this larger study.

False discovery has long been a challenge in spike detection, and we acknowledge that our model trained on the limited samples does not fully address this issue. However, identifying key relevant channels can help reduce false discoveries. For instance, if the first two detected channels are those nearest to the eyes, the spike is more likely related to eye movements. Additionally, training the model on larger datasets, which we are currently preparing, could significantly lower the false discovery rate.

Acknowledgement

The computations were performed using research computing facilities offered by Information Technology Services, the University of Hong Kong and by the Department of Radiology, UCSF. The work of Wei and Shen is partially supported by a HKSAR UGC CRF grant (C7162-20G). The work of Fei Jiang is supported by NIH grants K25AG071840 and R01NS132766.

References

- Antoniades, A., Spyrou, L., Took, C. C. and Sanei, S. (2016), “Deep learning for epileptic intracranial eeg data”, *in* 2016 IEEE 26th International Workshop on Machine Learning for Signal Processing (MLSP), pp. 1–6.
- Baud, M. O., Kleen, J. K., Anumanchipalli, G. K., Hamilton, L. S., Tan, Y.-L., Knowlton, R. et al. (2018), “Unsupervised learning of spatiotemporal interictal discharges in focal epilepsy”, *Neurosurgery* **83**(4), 683–691.
- Chung, Y. G., Lee, W.-J., Na, S. M., Kim, H., Hwang, H., Yun, C.-H. et al. (2023), “Deep learning-based automated detection and multiclass classification of focal interictal epileptiform discharges in scalp electroencephalograms”, *Scientific Reports* **13**(1), 6755.
- Clarke, S., Karoly, P. J., Nurse, E., Seneviratne, U., Taylor, J., Knight-Sadler, R., Kerr, R., Moore, B., Hennessy, P., Mendis, D. et al. (2021), “Computer-assisted eeg diagnostic review for idiopathic generalized epilepsy”, *Epilepsy & Behavior* **121**, 106556.
- Ester, M., Kriegel, H.-P., Sander, J. and Xu, X. (1996), “A density-based algorithm for discovering clusters in large spatial databases with noise”, *in* Proceedings of the Second International Conference on Knowledge Discovery and Data Mining, KDD’96, AAAI Press, p. 226–231.
- Goelz, H., Jones, R. D. and Bones, P. J. (2000), “Wavelet analysis of transient biomedical signals and its application to detection of epileptiform activity in the eeg”, *Clinical electroencephalography* **31**(4), 181–191.
- Golmohammadi, M., Harati Nejad Torbati, A. H., Lopez de Diego, S., Obeid, I. and

- Picone, J. (2019), “Automatic analysis of eegs using big data and hybrid deep learning architectures”, *Frontiers in human neuroscience* **13**, 76.
- Harati, A., Golmohammadi, M., Lopez, S., Obeid, I. and Picone, J. (2015), “Improved eeg event classification using differential energy”, *in* 2015 IEEE Signal Processing in Medicine and Biology Symposium (SPMB), IEEE, pp. 1–4.
- Indiradevi, K., Elias, E., Sathidevi, P., Nayak, S. D. and Radhakrishnan, K. (2008), “A multi-level wavelet approach for automatic detection of epileptic spikes in the electroencephalogram”, *Computers in biology and medicine* **38**(7), 805–816.
- Jing, J., Sun, H., Kim, J. A., Herlopian, A., Karakis, I., Ng, M. et al. (2020), “Development of expert-level automated detection of epileptiform discharges during electroencephalogram interpretation”, *JAMA neurology* **77**(1), 103–108.
- Johansen, A. R., Jin, J., Maszczyk, T., Dauwels, J., Cash, S. S. and Westover, M. B. (2016), “Epileptiform spike detection via convolutional neural networks”, *in* 2016 IEEE International Conference on Acoustics, Speech and Signal Processing (ICASSP), IEEE, pp. 754–758.
- Lodder, S. S., Askamp, J. and van Putten, M. J. (2013), “Inter-ictal spike detection using a database of smart templates”, *Clinical neurophysiology* **124**(12), 2328–2335.
- Lopez, S., Gross, A., Yang, S., Golmohammadi, M., Obeid, I. and Picone, J. (2016), “An analysis of two common reference points for eegs”, *in* 2016 IEEE signal processing in medicine and biology symposium (SPMB), IEEE, pp. 1–5.
- McIntosh, W. C. and Das, J. M. (2019), *Temporal Seizure*, StatPearls.

- Medvedev, A., Agoureeva, G. and Murro, A. (2019), “A long short-term memory neural network for the detection of epileptiform spikes and high frequency oscillations”, *Scientific reports* **9**(1), 19374.
- Munia, M. S., Nourani, M., Harvey, J. and Dave, H. (2023), “Interictal epileptiform discharge detection using multi-head deep convolutional neural network”, *in* 2023 45th Annual International Conference of the IEEE Engineering in Medicine & Biology Society (EMBC), IEEE, pp. 1–4.
- Nonclercq, A. and Ercek, R. (2016), “Spikedet: a spm eeg spike detection toolbox”, <http://beams.ulb.ac.be/research-projects/spm-eeg-spike-detection-toolbox>.
- Nonclercq, A., Foulon, M., Verheulpen, D., De Cock, C., Buzatu, M., Mathys, P. et al. (2009), “Spike detection algorithm automatically adapted to individual patients applied to spike and wave percentage quantification”, *Neurophysiologie Clinique/Clinical Neurophysiology* **39**(2), 123–131.
- Obeid, I. and Picone, J. (2016), “The temple university hospital eeg data corpus”, *Frontiers in neuroscience* **10**, 195498.
- Schmidt-Hieber, J. (2020), “Nonparametric regression using deep neural networks with ReLU activation function”, *The Annals of Statistics* **48**(4), 1875 – 1897.
URL: <https://doi.org/10.1214/19-AOS1875>
- Smith, E. H., Liou, J.-y., Merricks, E. M., Davis, T., Thomson, K., Greger, B. et al. (2022), “Human interictal epileptiform discharges are bidirectional traveling waves echoing ictal discharges”, *Elife* **11**, e73541.
- Thomas, J., Jin, J., Thangavel, P., Bagheri, E., Yuvaraj, R., Dauwels, J. et al. (2020),

“Automated detection of interictal epileptiform discharges from scalp electroencephalograms by convolutional neural networks”, *International journal of neural systems* **30**(11), 2050030.

Tjepkema-Cloostermans, M. C., de Carvalho, R. C. and van Putten, M. J. (2018), “Deep learning for detection of focal epileptiform discharges from scalp eeg recordings”, *Clinical neurophysiology* **129**(10), 2191–2196.

Torres, R. E. and Butter, I. H. (1996), “The impact of eeg technology on health manpower”, *American Journal of Electroneurodiagnostic Technology* **36**(2), 114–132.

Vershynin, R. (2010), “Introduction to the non-asymptotic analysis of random matrices”, *arXiv preprint arXiv:1011.3027*.

Wilson, S. B., Turner, C. A., Emerson, R. G. and Scheuer, M. L. (1999), “Spike detection ii: automatic, perception-based detection and clustering”, *Clinical neurophysiology* **110**(3), 404–411.

World Health Organization (2024), “Epilepsy”, <https://www.who.int/news-room/fact-sheets/detail/epilepsy>. Accessed: 2024-02-07.

Supplementary Materials for “Nested Deep Learning Model Towards a Foundation Model for Brain Signal Data.”

S1 Additional Notations

We write $a \lesssim b$ if there exists a constant C such that $a \leq Cb$ for all n . Moreover, $a \asymp b$ means that $a \lesssim b$ and $b \lesssim a$. Let $\mathcal{N}(\delta, \mathcal{F}, \|\cdot\|_\infty)$ be the covering number, that is, the minimal number of $\|\cdot\|_\infty$ -balls with radius δ that covers \mathcal{F} . For a variable X , we define $\|X\|_{\psi_2} = \sup_{k \geq 1} k^{-1/2}(E|X|^k)^{1/k}$ and define $\|X\|_{\psi_1} = \sup_{k \geq 1} k^{-1}(E|X|^k)^{1/k}$.

S2 Useful lemmas

Lemma S1 *Let \mathcal{F} be a sub-field of the sigma-field generated by X . Let $K_j(\mathcal{F}) > 0, j = 1, \dots, 4$ be functions of random variables in \mathcal{F} . Then, the following properties 1, 2, and 3 are equivalent, and when $E(X|\mathcal{F}) = 0$, they are further equivalent to property 4. In addition, $K_j(\mathcal{F})$ can be chosen to satisfy $0 < c < K_j(\mathcal{F})/K_k(\mathcal{F}) < C < \infty$, for all $k, j \in \{1, 2, 3, 4\}$, where c, C are absolute constants.*

1. *Tail: There exists $K_1(\mathcal{F})$ such that $\Pr(|X| > t|\mathcal{F}) \leq \exp\{1 - t^2/K_1^2(\mathcal{F})\}$;*
2. *Moments: There exists $K_2(\mathcal{F})$ such that $E(|X|^k|\mathcal{F})^{1/k} \leq K_2(\mathcal{F})\sqrt{k}$, for all $k \geq 1$;*
3. *Super-exponential moment: There exists $K_3(\mathcal{F})$ such that $E[\exp\{X^2/K_3^2(\mathcal{F})\}|\mathcal{F}] \leq e$;*
4. *Let $E(X|\mathcal{F}) = 0$. There exists $K_4(\mathcal{F})$ such that $E\{\exp(tX)|\mathcal{F}\} \leq \exp\{t^2 K_4^2(\mathcal{F})\}$.*

Definition 2 *A random variable X that satisfies one of the equivalent properties in Lemma S1 is named a conditional sub-Gaussian random variable with respect to the sub-sigma field*

\mathcal{F} . The conditional sub-gaussian norm of X with respect to \mathcal{F} , denoted by $\|X\|_{\psi_2(\mathcal{F})}$, is defined as the smallest $K_2(\mathcal{F})$ in property 2. That is,

$$\|X\|_{\psi_2(\mathcal{F})} = \sup_{k \geq 1} k^{-1/2} E(|X|^k | \mathcal{F})^{1/k}.$$

Lemma S2 Assume $f \in \mathcal{G}(q, \mathbf{d}, \mathbf{t}, \boldsymbol{\beta}, K)$. Furthermore, let $\beta_i^* \equiv \beta_i \prod_{l=i+1}^q \{\min(\beta_l, 1)\}$ and $\phi_n \equiv \max_{i=0, \dots, q} n^{-2\beta_i^*/(2\beta_i^*+t_i)}$. Define a function space $\mathcal{F}(L, (p_{wu})_{u=0, \dots, L+1}, s, F)$ satisfying the following conditions:

(i) $F \geq \max(K, 1)$,

(ii) $\sum_{i=0}^q \log_2 \{\max(4t_i, 4\beta_i)\} \log_2 n \leq L \lesssim n\phi_n$,

(iii) $n\phi_n \lesssim \min_{u=1, \dots, L} p_{wu}$,

(iv) $s \asymp n\phi_n \log n$.

Then there exists a $f_0 \in \mathcal{F}(L, (p_{wu})_{u=0, \dots, L+1}, s, F)$ such that

$$\|f_0 - f\|_{\infty}^2 \leq C \max_{v=0, \dots, q} c^{-\frac{2\beta_v^*}{t_v}} n^{-\frac{2\beta_v^*}{2\beta_v^*+t_v}}.$$

where C, c are constants only depends on $q, \mathbf{d}, \mathbf{t}, \boldsymbol{\beta}$.

Proof: This lemma is a direct consequence of (26) in Schmidt-Hieber (2020).

Lemma S3 For any $\delta > 0$, we have

$$\log \mathcal{N} \{ \delta, \mathcal{F}(L, \mathbf{p}_w, s, \infty), \|\cdot\|_{\infty} \} \leq (s+1) \log \{ 2^{2L+5} \delta^{-1} (L+1) p_{w0}^2 p_{wL+1}^2 s^{2L} \}.$$

Proof: This lemma is a direct consequence of Lemma 4 in Schmidt-Hieber (2020).

Lemma S4 Let X_1, \dots, X_N be independent centered sub-Gaussian random variable, and let $K = \max_i \|X_i\|_{\psi_2}$. Then for every $\mathbf{a} = (a_1, \dots, a_N)^\top \in \mathbb{R}^N$ and every $t \geq 0$, we have

$$\Pr \left(\left| \sum_{i=1}^N a_i X_i \right| \right) \leq e \cdot \exp \left(-\frac{ct^2}{K^2 \|\mathbf{a}\|_2^2} \right),$$

where $c > 0$ is an absolute constant.

Proof: This is a direct consequence of Proposition 5.10 in Vershynin (2010).

Lemma S5 *Let X_1, \dots, X_N be independent centered sub-exponential random variables, and $K = \max_i \|X_i\|_{\psi_1}$. Then for every $\mathbf{a} = (a_1, \dots, a_N)^\top \in \mathbb{R}^N$ and every $t > 0$, we have*

$$\Pr \left(\left| \sum_{i=1}^N a_i X_i \right| \right) \leq 2 \exp \left\{ -c \min \left(\frac{t^2}{K^2 \|\mathbf{a}\|_2^2}, \frac{t}{K \|\mathbf{a}\|_\infty} \right) \right\},$$

where $c > 0$ is an absolute constant.

S3 Proof of Proposition 1

Proof: For notation simplicity, we omit index i in the following proofs. If $\boldsymbol{\alpha}(\mathbf{X}_l, \mathbf{X})$ and the conditional density function $g\{\mathbf{S}(\boldsymbol{\alpha})\}$ are not identifiable, then we will have $\tilde{g}, \tilde{\boldsymbol{\alpha}}$ such that $(g, \boldsymbol{\alpha}) \neq (\tilde{g}, \tilde{\boldsymbol{\alpha}})$, but

$$\begin{aligned} & g \left\{ \sum_{l=1}^d \mathbf{X}_l \boldsymbol{\alpha}(\mathbf{X}_l, \mathbf{X})^\top + \mathbf{1}_T \boldsymbol{\alpha}(\mathbf{X}_l, \mathbf{X})^\top \mathbf{Z}_l \mathbf{1}_p^\top \right\} \\ &= \tilde{g} \left\{ \sum_{l=1}^d \mathbf{X}_l \tilde{\boldsymbol{\alpha}}(\mathbf{X}_l, \mathbf{X})^\top + \mathbf{1}_T \tilde{\boldsymbol{\alpha}}(\mathbf{X}_l, \mathbf{X})^\top \mathbf{Z}_l \mathbf{1}_p^\top \right\} \end{aligned} \quad (\text{S1})$$

for any given $\mathbf{X}_l, \mathbf{Z}_l$. Now replacing \mathbf{Z}_l by $\mathbf{Z}_l + \xi I(\mathbf{X}_l = \mathbf{X}_u) \mathbf{e}_j$ in (S1) where \mathbf{e}_j is a length p unit vector with the j th element 1, and $I(\cdot)$ is an indicator function, Taking the derivative of both sides with respect to ξ and evaluate at $\xi = 0$, denote \mathbf{M}_{qt} be the q, t th entry of matrix, \mathbf{M} , then the left-hand side follows

$$\begin{aligned} & \frac{\partial f \left\{ \sum_{l=1}^d \mathbf{X}_l \boldsymbol{\alpha}(\mathbf{X}_l, \mathbf{X})^\top + \mathbf{1}_T \boldsymbol{\alpha}(\mathbf{X}_l, \mathbf{X})^\top \{ \mathbf{Z}_l + \xi I(\mathbf{X}_l = \mathbf{X}_u) \mathbf{e}_j \} \mathbf{1}_p^\top \right\}}{\partial \xi} \Big|_{\xi=0} \\ &= \sum_{q=1}^p \sum_{t=1}^T \frac{\partial g \left\{ \sum_{l=1}^d \mathbf{X}_l \boldsymbol{\alpha}(\mathbf{X}_l, \mathbf{X})^\top + \mathbf{1}_T \boldsymbol{\alpha}(\mathbf{X}_l, \mathbf{X})^\top \mathbf{Z}_l \mathbf{1}_p^\top \right\}}{\partial \left\{ \sum_{l=1}^d \mathbf{X}_l \boldsymbol{\alpha}(\mathbf{X}_l, \mathbf{X})^\top + \mathbf{1}_T \boldsymbol{\alpha}(\mathbf{X}_l, \mathbf{X})^\top \mathbf{Z}_l \mathbf{1}_p^\top \right\}_{qt}} \sum_{l=1}^d \boldsymbol{\alpha}(\mathbf{X}_l, \mathbf{X})^\top \mathbf{e}_j I(\mathbf{X}_l = \mathbf{X}_u) \\ &= \sum_{q=1}^p \sum_{t=1}^T \frac{\partial g \left\{ \sum_{l=1}^d \mathbf{X}_l \boldsymbol{\alpha}(\mathbf{X}_l, \mathbf{X})^\top + \mathbf{1}_T \boldsymbol{\alpha}(\mathbf{X}_l, \mathbf{X})^\top \mathbf{Z}_l \mathbf{1}_p^\top \right\}}{\partial \left\{ \sum_{l=1}^d \mathbf{X}_l \boldsymbol{\alpha}(\mathbf{X}_l, \mathbf{X})^\top + \mathbf{1}_T \boldsymbol{\alpha}(\mathbf{X}_l, \mathbf{X})^\top \mathbf{Z}_l \mathbf{1}_p^\top \right\}_{qt}} \alpha_j(\mathbf{X}_u, \mathbf{X}). \end{aligned}$$

The same follows for the right-hand side, and hence we have

$$\sum_{q=1}^p \sum_{t=1}^T \frac{\partial g\{\mathbf{S}(\boldsymbol{\alpha})\}}{\partial S_{qt}(\boldsymbol{\alpha})} \alpha_j(\mathbf{X}_u, \mathbf{X}) = \sum_{q=1}^p \sum_{t=1}^T \frac{\partial \tilde{g}\{\mathbf{S}(\tilde{\boldsymbol{\alpha}})\}}{\partial S_{qt}(\tilde{\boldsymbol{\alpha}})} \tilde{\alpha}_j(\mathbf{X}_u, \mathbf{X}).$$

Now summing across \mathbf{u} , noting that $\partial g\{\mathbf{S}(\boldsymbol{\alpha})\}/\partial S_{qt}(\boldsymbol{\alpha})$, $\partial \tilde{g}\{\mathbf{S}(\tilde{\boldsymbol{\alpha}})\}/\partial S_{qt}(\tilde{\boldsymbol{\alpha}})$ do not contain \mathbf{X}_u , and $\sum_{u=1}^d \alpha_j(\mathbf{X}_u, \mathbf{X}) = \sum_{u=1}^d \tilde{\alpha}_j(\mathbf{X}_u, \mathbf{X}) = 1$ by our assumption, we obtain

$$\sum_{q=1}^p \sum_{t=1}^T \frac{\partial g\{\mathbf{S}(\boldsymbol{\alpha})\}}{\partial S_{qt}(\boldsymbol{\alpha})} = \sum_{q=1}^p \sum_{t=1}^T \frac{\partial g\{\mathbf{S}(\tilde{\boldsymbol{\alpha}})\}}{\partial S_{qt}(\tilde{\boldsymbol{\alpha}})}.$$

And hence we have

$$\alpha_j(\mathbf{X}_u, \mathbf{X}) = \tilde{\alpha}_j(\mathbf{X}_u, \mathbf{X}), j = 1, \dots, p,$$

for any \mathbf{X} and any \mathbf{u} . Combined with (S1), this suggests

$$g\{\mathbf{S}(\boldsymbol{\alpha})\} = \tilde{g}\{\mathbf{S}(\boldsymbol{\alpha})\},$$

for all $\mathbf{X}_l, \mathbf{Z}_l$, which implies $g = \tilde{g}$. This contradicts with the assumption. Therefore, g and $\boldsymbol{\alpha}$ are identifiable.

S4 Proof of Lemma 1

Proof: First note that

$$\begin{aligned} \alpha_j(\mathbf{x}_l, \mathbf{x}) - \alpha_{0j}(\mathbf{x}_l, \mathbf{x}) &= \frac{\exp(\omega_j(\mathbf{x}_l))}{\sum_{l=1}^d \exp(\omega_j(\mathbf{x}_l))} - \frac{\exp(\omega_{0j}(\mathbf{x}_l))}{\sum_{l=1}^d \exp(\omega_{0j}(\mathbf{x}_l))} \\ &= \frac{\exp(\omega_j^\dagger(\mathbf{x}_l))}{\sum_{l=1}^d \exp(\omega_j^\dagger(\mathbf{x}_l))} \left\{ \left(1 - \frac{\exp(\omega_j^\dagger(\mathbf{x}_l))}{\sum_{l=1}^d \exp(\omega_j^\dagger(\mathbf{x}_l))} \right) \{\omega_j(\mathbf{x}_l) - \omega_{0j}(\mathbf{x}_l)\} \right. \\ &\quad \left. - \sum_{u \neq l} \frac{\exp(\omega_j^\dagger(\mathbf{x}_u))}{\sum_{l=1}^d \exp(\omega_j^\dagger(\mathbf{x}_l))} \{\omega_j(\mathbf{x}_u) - \omega_{0j}(\mathbf{x}_u)\} \right\}, \end{aligned}$$

where ω_j^\dagger is one the line between ω_0 and ω_j , which implies

$$\sup_{\mathbf{X}_{il}, \mathbf{X}_i} |\alpha_j(\mathbf{X}_{il}, \mathbf{X}_i) - \alpha_{0j}(\mathbf{X}_{il}, \mathbf{X}_i)| \leq 2 \sup_{\mathbf{X}_{il}} |\{\omega_j(\mathbf{X}_{il}) - \omega_{0j}(\mathbf{X}_{il})\}|.$$

Furthermore,

$$\|\nabla_{g_0} \{\mathbf{S}_i(\boldsymbol{\alpha}_0)\}\|_2 \leq \|\mathbf{W}_{gL} \mathbf{W}_{gL-1}, \dots, \mathbf{W}_{g0}\|_2 \leq \sqrt{\prod_{l=1}^L s_{gl}},$$

where $\mathbf{W}_{gl}, l = 0, \dots, L$ are the weights for constructing g_0 , and s_{gl} is the sparseness of \mathbf{W}_{gl} . By the relationship between geometric and arithmetic means, we have $\prod_{l=1}^{L_g} s_{gl} \leq (\sum_{l=1}^{L_g} s_{gl}/L_g)^{L_g}$, which leads

$$\|\nabla_{g_0} \{\mathbf{S}_i(\boldsymbol{\alpha}_0)\}\|_2 \leq (s_g/L_g)^{L_g/2} \leq M_L. \quad (\text{S2})$$

The last inequality holds by Condition (C4). Moreover, because $\nabla_{jt} g_0 \{\mathbf{S}_i(\boldsymbol{\alpha}_0)\}$ has at most s_g nonzero elements,

$$\begin{aligned} & \left| \sum_{j=1}^p \sum_{t=1}^T \nabla_{jt} g_0 \{\mathbf{S}_i(\boldsymbol{\alpha}_0)\} \sum_{l=1}^d (X_{ilt} + Z_{ilj}) \{\alpha_j^*(\mathbf{X}_{il}, \mathbf{X}_i)^\top - \alpha_{j0}(\mathbf{X}_{il}, \mathbf{X}_i)^\top\} \right| \\ & \leq 2C_M M_L \sqrt{d \min(s_g, Tp)} \sup_{\mathbf{X}_i, j=1, \dots, p} |\alpha_j^*(\mathbf{X}_{il}, \mathbf{X}_i) - \alpha_{j0}(\mathbf{X}_{il}, \mathbf{X}_i)|. \end{aligned}$$

Therefore, by Lemma S2, we have

$$\begin{aligned} & |h' [g^* \{\mathbf{S}_i(\boldsymbol{\alpha}^*)\}] - h' [g_0 \{\mathbf{S}_i(\boldsymbol{\alpha}_0)\}]| \\ & = \left| h'' [g^\dagger \{\mathbf{S}_i(\boldsymbol{\alpha}^\dagger)\}] [g^* \{\mathbf{S}_i(\boldsymbol{\alpha}_0)\} - g_0 \{\mathbf{S}_i(\boldsymbol{\alpha}_0)\}] + h'' [g^\dagger \{\mathbf{S}_i(\boldsymbol{\alpha}^\dagger)\}] \right. \\ & \quad \times \left. \sum_{j=1}^p \sum_{t=1}^T \nabla_{jt} g^\dagger \{\mathbf{S}_i(\boldsymbol{\alpha}^\dagger)\} \sum_{l=1}^d (X_{ilt} + Z_{ilj}) \{\alpha_j^*(\mathbf{X}_{il}, \mathbf{X}_i)^\top - \alpha_{j0}(\mathbf{X}_{il}, \mathbf{X}_i)^\top\} \right| \\ & \leq \left\{ C_g \max_{u=0, \dots, q_g} c_g \frac{\beta_{gu}^*}{t_{gu}} n^{-\frac{\beta_{gu}^*}{2\beta_{gu}^* + t_{gu}}} + 2C_M M_L \sqrt{d \min(s_g, Tp)} \right. \\ & \quad \left. \sup_{j=1, \dots, p} C_{\omega_j} \max_{u=0, \dots, q_{\omega_j}} c_{\omega_j} \frac{\beta_{\omega_j u}^*}{t_{\omega_j u}} n^{-\frac{\beta_{\omega_j u}^*}{2\beta_{\omega_j u}^* + t_{\omega_j u}}} \right\}. \end{aligned}$$

S5 Useful Lemmas for Theorem 1

Lemma S6 Let $\psi_{\hat{g}} = \hat{g} - g_0$ and $\psi_{\hat{\alpha}_j} = \hat{\alpha}_j - \alpha_{0j}$. Assume $\hat{\alpha}_j, \alpha_{0j} \in \mathcal{H}_j$, $\omega_j^* \in \mathcal{G}_{\omega_j}$, and $\hat{g}, g_0 \in \mathcal{F}_g$, and $g^* \in \mathcal{G}_g$ and Conditions (C1)–(C6) hold, and $T, p \leq s_g$. Then we have there

are positive constants $C_g, C_{\omega_j}, c_g, c_{\omega_j}$, $\mathbf{C}_\omega = (C_{\omega_j}, j = 1, \dots, p)^\top$, $\mathbf{c}_\omega = (c_{\omega_j}, j = 1, \dots, p)^\top$

such that

$$\begin{aligned} & \left| n^{-1} \sum_{i=1}^n \left\{ (Y_i - h' [g_0 \{\mathbf{S}_i(\boldsymbol{\alpha}_0)\}]) \right. \right. \\ & \quad \left. \left. \sum_{j=1}^p \sum_{t=1}^T \nabla_{jt} g_0 \{\mathbf{S}_i(\boldsymbol{\alpha}_0)\} \sum_{l=1}^d (X_{ilt} + Z_{ilj}) \psi_{\hat{h}_j}(\mathbf{X}_{il}, \mathbf{X}_i) \right\} \right| \\ & \leq 4C_M M_L \eta(C_g, \mathbf{C}_\omega, c_g, \mathbf{c}_\omega) \left(\left[dpE \left\{ \sum_{j=1}^p \sum_{l=1}^d \{\sqrt{T} \psi_{\hat{\alpha}_j}(\mathbf{X}_{il}, \mathbf{X}_i)\}^2 \right\} \right]^{1/2} \right. \\ & \quad \left. + \min(s_g, Tp)^{1/2} \{\log(n)/(cn)\}^{1/4} \right) \end{aligned}$$

with probability greater than $1 - 6n^{-1}$. And there are positive constants $B_g, B_{\omega_j}, b_g, b_{\omega_j}$,

$\mathbf{B}_\omega = (B_{\omega_j}, j = 1, \dots, p)^\top$, $\mathbf{b}_\omega = (b_{\omega_j}, j = 1, \dots, p)^\top$ that

$$\begin{aligned} & \left| n^{-1} \sum_{i=1}^n \left\{ (Y_i - h' [g_0 \{\mathbf{S}_i(\boldsymbol{\alpha}_0)\}]) \psi_{\hat{g}} \{\mathbf{S}_i(\boldsymbol{\alpha}_0)\} \right\} \right| \\ & \leq 4C_M M_L \eta(B_g, B_g, \mathbf{B}_\omega, \mathbf{b}_\omega) \left[(E [\psi_{\hat{g}} \{\mathbf{S}_i(\boldsymbol{\alpha}_0)\}^2])^{1/2} + \{\log(n)/(cn)\}^{1/4} \right]. \end{aligned}$$

with probability greater than $1 - 6n^{-1}$.

Proof: Because $Y_i - h'[g^* \{\mathbf{S}_i(\boldsymbol{\alpha}^*)\}]$ is a sub-Gaussian random variable, by Lemma 1 that $|h'[g^* \{\mathbf{S}_i(\boldsymbol{\alpha}^*)\}] - h'[g_0 \{\mathbf{S}_i(\boldsymbol{\alpha}_0)\}]| \rightarrow 0$ almost surely, we have $Y_i - h'[g_0 \{\mathbf{S}_i(\boldsymbol{\alpha}_0)\}]$ is a sub-Gaussian random variable. Therefore using the concentration inequality in Lemma S4, we have

$$\begin{aligned} & \Pr \left[\left| n^{-1} \sum_{i=1}^n \left\{ (Y_i - h' [g_0 \{\mathbf{S}_i(\boldsymbol{\alpha}_0)\}]) - E(Y_i - h' [g_0 \{\mathbf{S}_i(\boldsymbol{\alpha}_0)\}]) \mid \mathcal{X}_n \right\} \right. \right. \\ & \quad \left. \left. \times \sum_{j=1}^p \sum_{t=1}^T \nabla_{jt} g_0 \{\mathbf{S}_i(\boldsymbol{\alpha}_0)\} \sum_{l=1}^d (X_{ilt} + Z_{ilj}) \psi_{\hat{\alpha}_j}(\mathbf{X}_{il}, \mathbf{X}_i) \right| \geq t \mid \mathcal{X}_n \right] \tag{S3} \\ & \leq 3 \exp \left(- \frac{nct^2}{16n^{-1} \sum_{i=1}^n \left[\sum_{j=1}^p \sum_{t=1}^T \nabla_{jt} g_0 \{\mathbf{S}_i(\boldsymbol{\alpha}_0)\} \sum_{l=1}^d (X_{ilt} + Z_{ilj}) \psi_{\hat{\alpha}_j}(\mathbf{X}_{il}, \mathbf{X}_i) \right]^2} \right). \end{aligned}$$

Let

$$t = \sqrt{C_0 \log(n)/(cn)} \left(n^{-1} \sum_{i=1}^n \left[\sum_{j=1}^p \sum_{t=1}^T \nabla_{jt} g_0 \{ \mathbf{S}_i(\boldsymbol{\alpha}_0) \} \sum_{l=1}^d (X_{ilt} + Z_{ilj}) \psi_{\hat{\alpha}_j}(\mathbf{X}_{il}, \mathbf{X}_i) \right]^2 \right)^{1/2},$$

where $C_0 = 16$, we obtain

$$\begin{aligned} & \left| n^{-1} \sum_{i=1}^n \{ (Y_i - h' [g_0 \{ \mathbf{S}_i(\boldsymbol{\alpha}_0) \}]) - E(Y_i - h' [g_0 \{ \mathbf{S}_i(\boldsymbol{\alpha}_0) \}] | \mathcal{X}_n) \} \right. \\ & \left. \sum_{j=1}^p \sum_{t=1}^T \nabla_{jt} g_0 \{ \mathbf{S}_i(\boldsymbol{\alpha}_0) \} \sum_{l=1}^d (X_{ilt} + Z_{ilj}) \psi_{\hat{\alpha}_j}(\mathbf{X}_{il}, \mathbf{X}_i) \right| \tag{S4} \\ & \leq \sqrt{C_0 \log(n)/(cn)} \left(n^{-1} \sum_{i=1}^n \left[\sum_{j=1}^p \sum_{t=1}^T \nabla_{jt} g_0 \{ \mathbf{S}_i(\boldsymbol{\alpha}_0) \} \sum_{l=1}^d (X_{ilt} + Z_{ilj}) \psi_{\hat{\alpha}_j}(\mathbf{X}_{il}, \mathbf{X}_i) \right]^2 \right)^{1/2} \end{aligned}$$

with probability greater than $1 - 3n^{-1}$.

Furthermore, Lemma 1 leads to

$$\begin{aligned} & \left| n^{-1} \sum_{i=1}^n E \{ (Y_i - h' [g_0 \{ \mathbf{S}_i(\boldsymbol{\alpha}_0) \}]) | \mathcal{X}_n \} \right. \\ & \left. \sum_{j=1}^p \sum_{t=1}^T \nabla_{jt} g_0 \{ \mathbf{S}_i(\boldsymbol{\alpha}_0) \} \sum_{l=1}^d (X_{ilt} + Z_{ilj}) \psi_{\hat{\alpha}_j}(\mathbf{X}_{il}, \mathbf{X}_i) \right| \\ & = \left| n^{-1} \sum_{i=1}^n \left\{ (h' [g^* \{ \mathbf{S}_i(\boldsymbol{\alpha}^*) \}]) - h' [g_0 \{ \mathbf{S}_i(\boldsymbol{\alpha}_0) \}]) \right. \right. \\ & \left. \left. \sum_{j=1}^p \sum_{t=1}^T \nabla_{jt} g_0 \{ \mathbf{S}_i(\boldsymbol{\alpha}_0) \} \sum_{l=1}^d (X_{ilt} + Z_{ilj}) \psi_{\hat{\alpha}_j}(\mathbf{X}_{il}, \mathbf{X}_i) \right\} \right| \\ & \leq \left\{ C_g \max_{u=0, \dots, q_g} c_g^{-\frac{\beta_{gu}^*}{t_{gu}}} n^{-\frac{\beta_{gu}^*}{2\beta_{gu}^* + t_{gu}}} + 2C_M M_L \sqrt{d \min(s_g, T p)} \right. \\ & \left. \sup_{j=1, \dots, p} C_{\omega_j} \max_{u=0, \dots, q_{\omega_j}} c_{\omega_j}^{-\frac{\beta_{\omega_j u}^*}{t_{\omega_j u}}} n^{-\frac{\beta_{\omega_j u}^*}{2\beta_{\omega_j u}^* + t_{\omega_j u}}} \right\} \\ & \left(n^{-1} \sum_{i=1}^n \left[\sum_{j=1}^p \sum_{t=1}^T \nabla_{jt} g_0 \{ \mathbf{S}_i(\boldsymbol{\alpha}_0) \} \sum_{l=1}^d (X_{ilt} + Z_{ilt}) \psi_{\hat{\alpha}_j}(\mathbf{X}_{il}, \mathbf{X}_i) \right]^2 \right)^{1/2}. \end{aligned}$$

Combine with (S4), we obtain there are positive constants $C_g, C_{\omega_j}, c_g, c_{\omega_j}$ such that

$$\left| n^{-1} \sum_{i=1}^n \left\{ (Y_i - h' [g_0 \{ \mathbf{S}_i(\boldsymbol{\alpha}_0) \}]) \right. \right.$$

$$\begin{aligned}
& \left. \sum_{j=1}^p \sum_{t=1}^T \nabla_{jt} g_0 \{ \mathbf{S}_i(\boldsymbol{\alpha}_0) \} \sum_{l=1}^d (X_{ilt} + Z_{ilj}) \psi_{\hat{\alpha}_j}(\mathbf{X}_{il}, \mathbf{X}_i) \right\} \Big| \\
& \leq \eta(C_g, \mathbf{C}_\omega, c_g, \mathbf{c}_\omega) \left(n^{-1} \sum_{i=1}^n \left[\sum_{j=1}^p \sum_{t=1}^T \nabla_{jt} g_0 \{ \mathbf{S}_i(\boldsymbol{\alpha}_0) \} \right. \right. \\
& \quad \left. \left. \times \sum_{l=1}^d (X_{ilt} + Z_{ilj}) \psi_{\hat{\alpha}_j}(\mathbf{X}_{il}, \mathbf{X}_i) \right]^2 \right)^{1/2}, \tag{S5}
\end{aligned}$$

with probability greater than $1 - 3n^{-1}$. Additionally, because $\nabla g_0 \{ \mathbf{S}_i(\boldsymbol{\alpha}_0) \}$ is s_g sparse and $\sum_{l=1}^d \hat{\alpha}_j(\mathbf{X}_{il}, \mathbf{X}_i) = \sum_{l=1}^d \alpha_{0j}(\mathbf{X}_{il}, \mathbf{X}_i) = 1$, we have

$$\left| \sum_{j=1}^p \sum_{t=1}^T \nabla_{jt} g_0 \{ \mathbf{S}_i(\boldsymbol{\alpha}_0) \} \sum_{l=1}^d (X_{ilt} + Z_{ilj}) \psi_{\hat{\alpha}_j}(\mathbf{X}_{il}, \mathbf{X}_i) \right| \leq 4C_M M_L \sqrt{\min(s_g, Tp)}.$$

Therefore $\left\{ \sum_{j=1}^p \sum_{t=1}^T \nabla_{jt} g_0 \{ \mathbf{S}_i(\boldsymbol{\alpha}_0) \} \sum_{l=1}^d (X_{ilt} + Z_{ilj}) \psi_{\hat{\alpha}_j}(\mathbf{X}_{il}, \mathbf{X}_i) \right\}^2 / \min(s_g, Tp)$ is sub-Gaussian variable, and hence

$$\begin{aligned}
& \Pr \left\{ \left| n^{-1} \min(s_g, Tp)^{-1} \sum_{i=1}^n \left[\sum_{j=1}^p \sum_{t=1}^T \nabla_{jt} g_0 \{ \mathbf{S}_i(\boldsymbol{\alpha}_0) \} \sum_{l=1}^d (X_{il} + Z_{ilj}) \psi_{\hat{\alpha}_j}(\mathbf{X}_{il}, \mathbf{X}_i) \right]^2 \right. \right. \\
& \quad \left. \left. - \min(s_g, Tp)^{-1} E \left(\left[\sum_{j=1}^p \sum_{t=1}^T \nabla_{jt} g_0 \{ \mathbf{S}_i(\boldsymbol{\alpha}_0) \} \sum_{l=1}^d (X_{il} + Z_{ilj}) \psi_{\hat{\alpha}_j}(\mathbf{X}_{il}, \mathbf{X}_i) \right]^2 \right) \right| > t \right\} \\
& \leq 3 \exp \{ -cnt^2 / (256C_M^4 M_L^4) \}.
\end{aligned}$$

Let $t = \sqrt{256M_L^4 C_M^4 \log(n) / (cn)}$, we have

$$\begin{aligned}
& \left| n^{-1} \sum_{i=1}^n \left\{ \sum_{j=1}^p \sum_{t=1}^T \nabla_{jt} g_0 \{ \mathbf{S}_i(\boldsymbol{\alpha}_0) \} \sum_{l=1}^d (X_{ilt} + Z_{ilj}) \psi_{\hat{\alpha}_j}(\mathbf{X}_{il}, \mathbf{X}_i) \right\}^2 \right. \\
& \quad \left. - E \left(\left\{ \sum_{j=1}^p \sum_{t=1}^T \nabla_{jt} g_0 \{ \mathbf{S}_i(\boldsymbol{\alpha}_0) \} \sum_{l=1}^d (X_{il} + Z_{ilj}) \psi_{\hat{\alpha}_j}(\mathbf{X}_{il}, \mathbf{X}_i) \right\}^2 \right) \right| \\
& \leq 16 \min(s_g, Tp) C_M^2 M_L^2 \sqrt{\log(n) / (cn)}, \tag{S6}
\end{aligned}$$

with probability greater than $1 - 3/n$. Next

$$E \left(\left[\sum_{j=1}^p \sum_{t=1}^T \nabla_{jt} g_0 \{ \mathbf{S}_i(\boldsymbol{\alpha}_0) \} \sum_{l=1}^d (X_{ilt} + Z_{ilj}) \psi_{\hat{\alpha}_j}(\mathbf{X}_{il}, \mathbf{X}_i) \right]^2 \right)$$

$$\begin{aligned}
&\leq E \left(\left[\left| \sup_{l=1, \dots, d, j=1, \dots, p} \sum_{t=1}^T \nabla_{jt} g_0 \{ \mathbf{S}_i(\boldsymbol{\alpha}_0) \} (X_{ilt} + Z_{ilj}) / \sqrt{T} \right| \right. \right. \\
&\quad \left. \left. \times \sum_{j=1}^p \sum_{l=1}^d \left| \sqrt{T} \psi_{\hat{\alpha}_j}(\mathbf{X}_{il}, \mathbf{X}_i) \right| \right]^2 \right) \\
&\leq 4C_M^2 M_L^2 E \left\{ \left(\sqrt{dp} \left[\sum_{j=1}^p \sum_{l=1}^d \left\{ \sqrt{T} \psi_{\hat{\alpha}_j}(\mathbf{X}_{il}, \mathbf{X}_i) \right\}^2 \right]^{1/2} \right)^2 \right\} \\
&= 4C_M^2 M_L^2 dp E \left[\sum_{j=1}^p \sum_{l=1}^d \left\{ \sqrt{T} \psi_{\hat{\alpha}_j}(\mathbf{X}_{il}, \mathbf{X}_i) \right\}^2 \right],
\end{aligned}$$

for a constant C_M , where the second inequality holds because

$$\begin{aligned}
&\left| \sup_{l=1, \dots, d, j=1, \dots, p} \sum_{t=1}^T \nabla_{jt} g_0 \{ \mathbf{S}_i(\boldsymbol{\alpha}_0) \} (X_{ilt} + Z_{ilj}) \right| \\
&\leq 2C_M \sup_{l=1, \dots, d, j=1, \dots, p} \sum_{t=1}^T |\nabla_{jt} g_0 \{ \mathbf{S}_i(\boldsymbol{\alpha}_0) \}| \\
&\leq 2C_M \sqrt{T} \sup_{l=1, \dots, d, j=1, \dots, p} \left[\sum_{t=1}^T |\nabla_{jt} g_0 \{ \mathbf{S}_i(\boldsymbol{\alpha}_0) \}| \right]^{1/2} \\
&\leq 2C_M \sqrt{T} M_L,
\end{aligned}$$

by (S2). Plugging the above inequality and (S6) to (S5), we obtain

$$\begin{aligned}
&\left| n^{-1} \sum_{i=1}^n \{ (Y_i - h' [g_0 \{ \mathbf{S}_i(\boldsymbol{\alpha}_0) \}]) \right. \\
&\quad \left. \sum_{j=1}^p \sum_{t=1}^T \nabla_{jt} g_0 \{ \mathbf{S}_i(\boldsymbol{\alpha}_0) \} \sum_{l=1}^d (X_{ilt} + Z_{ilj}) \psi_{\hat{\alpha}_j}(\mathbf{X}_{il}, \mathbf{X}_i) \right\} \Big| \\
&\leq \eta(C_g, \mathbf{C}_\omega, c_g, \mathbf{c}_\omega) \left(2C_M M_L \left[dp E \left\{ \sum_{j=1}^p \sum_{l=1}^d \left\{ \sqrt{T} \psi_{\hat{\alpha}_j}(\mathbf{X}_{il}, \mathbf{X}_i) \right\}^2 \right\} \right]^{1/2} \right. \\
&\quad \left. + 4C_M M_L \min(s_g, Tp)^{1/2} \{ \log(n)/(cn) \}^{1/4} \right) \\
&\leq 4C_M M_L \eta(C_g, \mathbf{C}_\omega, c_g, \mathbf{c}_\omega) \left(\left[dp E \left\{ \sum_{j=1}^p \sum_{l=1}^d \left\{ \sqrt{T} \psi_{\hat{\alpha}_j}(\mathbf{X}_{il}, \mathbf{X}_i) \right\}^2 \right\} \right]^{1/2} \right. \\
&\quad \left. + \min(s_g, Tp)^{1/2} \{ \log(n)/(cn) \}^{1/4} \right)
\end{aligned}$$

with probability greater than $1 - 6n^{-1}$. Using the same arguments and realize that we

obtain there are positive constants $B_g, B_{\omega_j}, b_g, b_{\omega_j}$ and realize that $\|\psi_{\hat{g}}\|_2 \leq 2C_M M_L$, we have

$$\begin{aligned} & \left| n^{-1} \sum_{i=1}^n \{(Y_i - h' [g_0 \{\mathbf{S}_i(\boldsymbol{\alpha}_0)\}]) \psi_{\hat{g}} \{\mathbf{S}_i(\boldsymbol{\alpha}_0)\}\} \right| \\ & \leq 4C_M M_L \eta(B_g, \mathbf{B}_\omega, b_g, \mathbf{B}_\omega) \left[(E [\psi_{\hat{g}} \{\mathbf{S}_i(\boldsymbol{\alpha}_0)\}^2])^{1/2} + \{\log(n)/(cn)\}^{1/4} \right]. \end{aligned}$$

with probability greater than $1 - 6n^{-1}$. This proves the result.

Lemma S7 Assume $\hat{\alpha}_j, \alpha_{0j} \in \mathcal{H}_j$, $\omega_j^* \in \mathcal{G}_{\omega_j}$, and $\hat{g}, g_0 \in \mathcal{F}_g$, $g^* \in \mathcal{G}_g$. Furthermore, assume Condition (C1)–(C7) hold, and $d/n \rightarrow 0$ and $T/n \rightarrow 0$ and $p < \infty$. Then for given $\epsilon_g^\dagger, \epsilon_{\alpha_j}^\dagger \in (0, 1)$, $\boldsymbol{\epsilon}_\alpha^\dagger = \{\epsilon_{\alpha_j}^\dagger, j = 1, \dots, p\}^\top$, we have

$$\begin{aligned} \Omega(g_0, \boldsymbol{\alpha}_0, \psi_{\hat{g}}, \boldsymbol{\psi}_{\hat{\alpha}}, \epsilon_g^\dagger, \boldsymbol{\epsilon}_\alpha^\dagger) & \geq \alpha_{\min} E \left[\psi_{\hat{g}} \{\mathbf{S}_i(\boldsymbol{\alpha}_0)\}^2 + \sum_{j=1}^p \sum_{l=1}^d T \psi_{\hat{\alpha}_j}(\mathbf{X}_{il}, \mathbf{X}_i)^2 \right] \\ & - 2TpC_1 \log^2(n) \left\{ \phi_{gn} L_g + \sum_{j=1}^p \phi_{\omega_j n} L_{\omega_j} \right\} - C_H Tp/n \end{aligned}$$

with probability greater than $1 - 2 \exp \left[-nC_1 \log^2(n) \left\{ \phi_{gn} L_g + \sum_{j=1}^p \phi_{\omega_j n} L_{\omega_j} \right\} \right]$ for some constants $C_H, C_1 > 0$.

Proof: Let $\psi_{\hat{g}} = \hat{g} - g_0$, $\psi_{\hat{\alpha}_k} = \hat{\alpha}_k - \alpha_0$. First, because $\hat{g}, g_0, \hat{\alpha}_k, \alpha_0$ are bounded functions, ∇g is bounded in the sense of S2, and Y_i is bounded, and $\|\mathbf{X}_{il}\|_2 \leq C_M \sqrt{T}$ by Condition (C5), it is easy to see that every summand in $Tp^{-1} \Omega(g_0, \boldsymbol{\alpha}_0, \psi_g, \boldsymbol{\psi}_\alpha, \epsilon_g^\dagger, \boldsymbol{\epsilon}_\alpha^\dagger)$ is a product of bounded sub-Gaussian variable, and hence sub-exponential. Therefore, by Lemma S5, for arbitrary $g, \boldsymbol{\alpha}$, there is a constant $c_H > 0$ such that

$$\begin{aligned} & \Pr \left\{ |(Tp)^{-1} \Omega(g_0, \boldsymbol{\alpha}_0, \psi_g, \boldsymbol{\psi}_\alpha, \epsilon_g^\dagger, \boldsymbol{\epsilon}_\alpha^\dagger) - (Tp)^{-1} E \{ \Omega(g_0, \boldsymbol{\alpha}_0, \psi_g, \boldsymbol{\psi}_\alpha, \epsilon_g^\dagger, \boldsymbol{\epsilon}_\alpha^\dagger) \}| > t \right\} \\ & \leq 3 \exp \{ -c_H n \min(t^2, t) \}. \end{aligned}$$

Let $\mathcal{S}_g(\delta)$ be the δ covering of \mathcal{F}_g and $\mathcal{S}_{\omega_k}(\delta)$ be the δ covering of \mathcal{F}_{ω_k} , then for some constant $C_H > 0$, we have

$$\Pr \left\{ \sup_{g \in \mathcal{F}_g, \alpha_k \in \mathcal{H}_k} |\Omega(g_0, \boldsymbol{\alpha}_0, \psi_g, \boldsymbol{\psi}_\alpha, \epsilon_g^\dagger, \boldsymbol{\epsilon}_\alpha^\dagger) - E \{ \Omega(g_0, \boldsymbol{\alpha}_0, \psi_g, \boldsymbol{\psi}_\alpha, \epsilon_g^\dagger, \boldsymbol{\epsilon}_\alpha^\dagger) \}| > Tpt + C_H Tp\delta \right\}$$

$$\begin{aligned}
&\leq \Pr \left\{ \max_{g \in \mathcal{S}_g, \omega_k \in \mathcal{S}_{\omega_k}} |\Omega(g_0, \boldsymbol{\alpha}_0, \psi_g, \boldsymbol{\psi}_\alpha, \epsilon_g^\dagger, \epsilon_\alpha^\dagger) - E\{\Omega(g_0, \boldsymbol{\alpha}_0, \psi_g, \boldsymbol{\psi}_\alpha, \epsilon_g^\dagger, \epsilon_\alpha^\dagger)\}| > Tpt \right\} \\
&\leq 2 \exp \left[-c_H n \min(t^2, t) + \log \mathcal{N} \{ \delta, \mathcal{F}_g, \|\cdot\|_\infty \} + \sum_{k=1}^p \log \mathcal{N} \{ \delta, \mathcal{F}_{\omega_k}, \|\cdot\|_\infty \} \right] \\
&\leq 2 \exp \left[-c_H n \min(t^2, t) + (s_g + 1) \log \left\{ 2^{2L_g+5} \delta^{-1} (L+1) p_{g0}^2 p_{gL_g+1}^2 s_g^{2L_g} \right\} \right. \\
&\quad \left. + \sum_{k=1}^p (s_{\omega_k} + 1) \log \left\{ 2^{2L_{\omega_k}+5} \delta^{-1} (L_g \omega_k + 1) p_{\omega_k 0}^2 p_{\omega_k L_{\omega_k}+1}^2 s_{\omega_k}^{2L_{\omega_k}} \right\} \right] \\
&\leq 2 \exp \left[-c_H n \min(t^2, t) + (s_g + 1) L_g \log \left\{ 2s_g \delta^{-1} (L_g + 1) d^2 p^2 s_g^{2L_g} \right\} \right. \\
&\quad \left. + \sum_{k=1}^p (s_{\omega_k} + 1) \log \left\{ 2^{2L_{\omega_k}+5} \delta^{-1} (L_{\omega_k} + 1) p_{\omega_k 0}^2 p_{\omega_k L_{\omega_k}+1}^2 s_{\omega_k}^{2L_{\omega_k}} \right\} \right].
\end{aligned}$$

Now plugging $\delta = n^{-1}$ using Condition (C2)–(C4) and the fact that $d/n \rightarrow 0$ and $T/n \rightarrow 0$ and $p < \infty$, we have

$$\begin{aligned}
&\Pr \left\{ \sup_{g \in \mathcal{F}_g, \alpha_k \in \mathcal{H}_k} |\Omega(g_0, \boldsymbol{\alpha}_0, \psi_g, \boldsymbol{\psi}_\alpha, \epsilon_g^\dagger, \epsilon_\alpha^\dagger) - E\{\Omega(g_0, \boldsymbol{\alpha}_0, \psi_g, \boldsymbol{\psi}_\alpha, \epsilon_g^\dagger, \epsilon_\alpha^\dagger)\}| > Tpt + C_H Tp/n \right\} \\
&\leq 2 \exp \left[-c_H n \min(t^2, t) + c_1 n \phi_{gn} L_g \log^2(n) + \sum_{j=1}^p c_{2j} n \phi_{\omega_j n} L_{\omega_j} \log^2(n) \right].
\end{aligned}$$

Let $t = \max \left[2C_1 \log^2(n) \left\{ \phi_{gn} L_g + \sum_{j=1}^p \phi_{\omega_j n} L_{\omega_j} \log^2(n) \right\}, 1 \right]$, where $C_1 = 2\{c_1 + \max_j(c_{2j})\}/c_H$, we have

$$\begin{aligned}
&\Pr \left\{ \sup_{g \in \mathcal{F}_g, \alpha_k \in \mathcal{H}_k} |\Omega(g_0, \boldsymbol{\alpha}_0, \psi_g, \boldsymbol{\psi}_\alpha, \epsilon_g^\dagger, \epsilon_\alpha^\dagger) - E\{\Omega(g_0, \boldsymbol{\alpha}_0, \psi_g, \boldsymbol{\psi}_\alpha, \epsilon_g^\dagger, \epsilon_\alpha^\dagger)\}| \right. \\
&\quad \left. > 2TpC_1 \log^2(n) \left\{ \phi_{gn} L_g + \sum_{j=1}^p \phi_{\omega_j n} L_{\omega_j} \right\} + C_H Tp/n \right\} \\
&\leq 2 \exp \left[-nC_1 \log^2(n) \left\{ \phi_{gn} L_g + \sum_{j=1}^p \phi_{\omega_j n} L_{\omega_j} \right\} \right].
\end{aligned}$$

Therefore,

$$\begin{aligned}
&|\Omega(g_0, \boldsymbol{\alpha}_0, \psi_{\hat{g}}, \boldsymbol{\psi}_{\hat{\alpha}}, \epsilon_g^\dagger, \epsilon_\alpha^\dagger) - E\{\Omega(g_0, \boldsymbol{\alpha}_0, \psi_{\hat{g}}, \boldsymbol{\psi}_{\hat{\alpha}}, \epsilon_g^\dagger, \epsilon_\alpha^\dagger)\}| \\
&\leq TpC_1 \log^2(n) \left\{ \phi_{gn} L_g + \sum_{j=1}^p \phi_{\omega_j n} L_{\omega_j} \right\} + C_H Tp/n,
\end{aligned}$$

with probability greater than $1 - 2 \exp \left[-nC_1 \log^2(n) \left\{ \phi_{gn}L_g + \sum_{j=1}^p \phi_{\omega_j n}L_{\omega_j} \right\} \right]$ for some $C_1 > 0$. Hence

$$\begin{aligned} \Omega(g_0, \boldsymbol{\alpha}_0, \psi_{\hat{g}}, \boldsymbol{\psi}_{\hat{\boldsymbol{\alpha}}}, \epsilon_g^\dagger, \boldsymbol{\epsilon}_\alpha^\dagger) &\geq \alpha_{\min} E \left[\psi_{\hat{g}} \{ \mathbf{S}_i(\boldsymbol{\alpha}_0) \}^2 + \sum_{j=1}^p \sum_{l=1}^d T \psi_{\hat{\alpha}_j}(\mathbf{X}_{il}, \mathbf{X}_i)^2 \right] \\ &- TpC_1 \log^2(n) \left\{ \phi_{gn}L_g + \sum_{j=1}^p \phi_{\omega_j n}L_{\omega_j} \right\} - C_H Tp/n \end{aligned}$$

with probability greater than $1 - 2 \exp \left[-nC_1 \log^2(n) \left\{ \phi_{gn}L_g + \sum_{j=1}^p \phi_{\omega_j n}L_{\omega_j} \right\} \right]$. This proves the result.

S6 Proof of Theorem 1

Proof: Because \hat{g} , $\hat{\boldsymbol{\alpha}}$ is the minimizer of (4), we have

$$\begin{aligned} 0 &\geq \mathcal{L}(\hat{g}, \hat{\boldsymbol{\alpha}}) - \mathcal{L}(g_0, \boldsymbol{\alpha}_0) \\ &= -n^{-1} \sum_{i=1}^n \left\{ (Y_i - h' [g_0 \{ \mathbf{S}_i(\boldsymbol{\alpha}_0) \}]) \right. \\ &\quad \left. \sum_{j=1}^p \sum_{t=1}^T \nabla_{jt} g_0 \{ \mathbf{S}_i(\boldsymbol{\alpha}_0) \} \sum_{l=1}^d (X_{ilt} + Z_{ilj}) \psi_{\hat{\alpha}_j}(\mathbf{X}_{il}, \mathbf{X}_i) \right\} \\ &\quad - n^{-1} \sum_{i=1}^n [(Y_i - h' [g_0 \{ \mathbf{S}_i(\boldsymbol{\alpha}_0) \}]) \psi_{\hat{g}} \{ \mathbf{S}_i(\boldsymbol{\alpha}_0) \}] \\ &\quad + \Omega(g_0, \boldsymbol{\alpha}_0, \psi_{\hat{g}}, \boldsymbol{\psi}_{\hat{\boldsymbol{\alpha}}}, \epsilon_g^\dagger, \boldsymbol{\epsilon}_\alpha^\dagger)/2, \end{aligned}$$

where $\epsilon_g^\dagger, \epsilon_{\alpha_j}^\dagger \in (0, 1)$ and $\boldsymbol{\epsilon}_\alpha^\dagger = (\epsilon_{\alpha_j}^\dagger, j = 1, \dots, p)^\top$. By Lemma S6 and S7, we have there are positive constants $D_g, d_g, \mathbf{D}_\omega = (D_{\omega_j}), \mathbf{d}_\omega = (d_{\omega_j})$ such that

$$\begin{aligned} &4C_M M_L \eta(D_g, d_g, \mathbf{D}_\omega, \mathbf{d}_\omega) \left[\left[dp E \left\{ \sum_{j=1}^p \sum_{l=1}^d T \psi_{\hat{\alpha}_j}(\mathbf{X}_{il}, \mathbf{X}_i)^2 \right\} \right]^{1/2} \right. \\ &+ \left. (E [\psi_{\hat{g}} \{ \mathbf{S}_i(\boldsymbol{\alpha}_0) \}^2])^{1/2} \right] + 4C_M M_L \eta(D_g, d_g, \mathbf{D}_\omega, \mathbf{d}_\omega) \left[\min(s_g, Tp)^{1/2} \{ \log(n)/(cn) \}^{1/4} \right. \\ &+ \left. \{ \log(n)/(cn) \}^{1/4} \right] + TpC_1 \log^2(n) \left\{ \phi_{gn}L_g + \sum_{j=1}^p \phi_{\omega_j n}L_{\omega_j} \right\} /2 + C_H Tp/(2n) \end{aligned}$$

$$\geq \alpha_{\min} E \left[\psi_{\hat{g}} \{ \mathbf{S}_i(\boldsymbol{\alpha}_0) \}^2 + \sum_{j=1}^p \sum_{l=1}^d T \psi_{\hat{\alpha}_j}(\mathbf{X}_{il}, \mathbf{X}_i)^2 \right] / 2$$

with probability greater than $1 - 6n^{-1} - 2 \exp \left[-nC_1 \log^2(n) \left\{ \phi_{gn} L_g + \sum_{j=1}^p \phi_{\omega_j n} L_{\omega_j} \right\} \right]$.

This implies

$$\begin{aligned} & 4C_M M_L \eta(D_g, d_g, \mathbf{D}_\omega, \mathbf{d}_\omega) (dp/2)^{1/2} \left(E \left\{ \sum_{j=1}^p \sum_{l=1}^d T \psi_{\hat{\alpha}_j}(\mathbf{X}_{il}, \mathbf{X}_i)^2 \right\} \right. \\ & \left. + E \left[\psi_{\hat{g}} \{ \mathbf{S}_i(\boldsymbol{\alpha}_0) \}^2 \right] \right)^{1/2} \\ & + 4C_M M_L \eta(D_g, d_g, \mathbf{D}_\omega, \mathbf{d}_\omega) \left[\min(s_g, Tp)^{1/2} \{ \log(n)/(cn) \}^{1/4} + \{ 16 \log(n)/(cn) \}^{1/4} \right] \\ & + TpC_1 \log^2(n) \left\{ \phi_{gn} L_g + \sum_{j=1}^p \phi_{\omega_j n} L_{\omega_j} \right\} / 2 + C_H Tp / (2n) \\ & \geq \alpha_{\min} E \left[\psi_{\hat{g}} \{ \mathbf{S}_i(\boldsymbol{\alpha}_0) \}^2 + \sum_{j=1}^p \sum_{l=1}^d T \psi_{\hat{\alpha}_j}(\mathbf{X}_{il}, \mathbf{X}_i)^2 \right] / 2. \end{aligned}$$

Therefore, we have

$$\begin{aligned} & E \left[\psi_{\hat{g}} \{ \mathbf{S}_i(\boldsymbol{\alpha}_0) \}^2 + \sum_{j=1}^p \sum_{l=1}^d T \psi_{\hat{\alpha}_j}(\mathbf{X}_{il}, \mathbf{X}_i)^2 \right] \\ & \leq 16\alpha_{\min}^{-1} \left(C_M M_L \eta(D_g, d_g, \mathbf{D}_\omega, \mathbf{d}_\omega) \left[\min(s_g, Tp)^{1/2} \{ \log(n)/(cn) \}^{1/4} + \{ \log(n)/(cn) \}^{1/4} \right] \right. \\ & \left. + TpC_1 \log^2(n) \left\{ \phi_{gn} L_g + \sum_{j=1}^p \phi_{\omega_j n} L_{\omega_j} \right\} / 2 + C_H Tp / (2n) \right) \\ & + 32C_M M_L dp \alpha_{\min}^{-2} \eta(D_g, d_g, \mathbf{D}_\omega, \mathbf{d}_\omega)^2. \end{aligned}$$

Now because $\|dP_{\boldsymbol{\alpha}_0}(\mathbf{z})/dP_{\boldsymbol{\alpha}^*}(\mathbf{z})\|_\infty \geq m_h$ almost surely, we obtain

$$\begin{aligned} & E \left[\psi_{\hat{g}} \{ \mathbf{S}_i(\boldsymbol{\alpha}^*) \}^2 + \sum_{j=1}^p \sum_{l=1}^d T \psi_{\hat{\alpha}_j}(\mathbf{X}_{il}, \mathbf{X}_i)^2 \right] \\ & \leq 16 \min(m_h, 1)^{-1} \alpha_{\min}^{-1} \left(C_M M_L \eta(D_g, d_g, \mathbf{D}_\omega, \mathbf{d}_\omega) \left[\min(s_g, Tp)^{1/2} \{ \log(n)/(cn) \}^{1/4} \right. \right. \\ & \left. \left. + \{ \log(n)/(cn) \}^{1/4} \right] + TpC_1 \log^2(n) \left\{ \phi_{gn} L_g + \sum_{j=1}^p \phi_{\omega_j n} L_{\omega_j} \right\} + C_H Tp / n \right) \\ & + 32 \min(m_h, 1)^{-1} C_M M_L dp \alpha_{\min}^{-2} \eta(D_g, d_g, \mathbf{D}_\omega, \mathbf{d}_\omega)^2. \end{aligned}$$

Now again using Lemma S2, we obtain there are constants D_{g1}, D_{ω_j1} such that

$$\int \{ \hat{g}(\mathbf{z}) - g^*(\mathbf{z}) \}^2 dP_{\boldsymbol{\alpha}^*}(\mathbf{z}) + T \sum_{j=1}^p \int \sum_{l=1}^d \{ \hat{\alpha}_j(\mathbf{x}_l, \mathbf{x}) - \alpha_j^*(\mathbf{x}_l, \mathbf{x}) \}^2 dP_{\mathbf{X}}(\mathbf{x})$$

$$\begin{aligned}
&\leq 16 \min(m_h, 1)^{-1} \alpha_{\min}^{-1} \left(C_M M_L \eta(D_g, d_g, \mathbf{D}_\omega, \mathbf{d}_\omega) \left[\min(s_g, Tp)^{1/2} \{\log(n)/(cn)\}^{1/4} \right. \right. \\
&\quad \left. \left. + \{\log(n)/(cn)\}^{1/4} \right] + Tp C_1 \log^2(n) \left\{ \phi_{gn} L_g + \sum_{j=1}^p \phi_{\omega_j n} L_{\omega_j} \right\} + C_H Tp/n \right) \\
&\quad + 32 \min(m_h, 1)^{-1} C_M M_L dp \alpha_{\min}^{-2} \eta(D_g, d_g, \mathbf{D}_\omega, \mathbf{d}_\omega)^2 + \left(D_{g1} \phi_{gn} + T \sum_{j=1}^p D_{\omega_j 1} \phi_{\omega_j n} \right)
\end{aligned}$$

with probability greater than $1 - 6n^{-1} - 2 \exp \left[-nC_1 \log^2(n) \left\{ \phi_{gn} L_g + \sum_{j=1}^p \phi_{\omega_j n} L_{\omega_j} \right\} \right]$.

This proves the result.

S7 The Standard ACNS Temporal Central Parasagittal (TCP) Montage

Table S1: The standard ACNS TCP montage.

Index	Montage	Anode	Cathode
0	FP1-F7	EEG FP1-REF	EEG F7-REF
1	F7-T3	EEG F7-REF	EEG T3-REF
2	T3-T5	EEG T3-REF	EEG T5-REF
3	T5-O1	EEG T5-REF	EEG O1-REF
4	FP2-F8	EEG FP2-REF	EEG F8-REF
5	F8-T4	EEG F8-REF	EEG T4-REF
6	T4-T6	EEG T4-REF	EEG T6-REF
7	T6-O2	EEG T6-REF	EEG O2-REF
8	A1-T3	EEG A1-REF	EEG T3-REF
9	T3-C3	EEG T3-REF	EEG C3-REF
10	C3-CZ	EEG C3-REF	EEG CZ-REF
11	CZ-C4	EEG CZ-REF	EEG C4-REF
12	C4-T4	EEG C4-REF	EEG T4-REF
13	T4-A2	EEG T4-REF	EEG A2-REF
14	FP1-F3	EEG FP1-REF	EEG F3-REF
15	F3-C3	EEG F3-REF	EEG C3-REF
16	C3-P3	EEG C3-REF	EEG P3-REF
17	P3-O1	EEG P3-REF	EEG O1-REF
18	FP2-F4	EEG FP2-REF	EEG F4-REF
19	F4-C4	EEG F4-REF	EEG C4-REF
20	C4-P4	EEG C4-REF	EEG P4-REF
21	P4-O2	EEG P4-REF	EEG O2-REF